SWELL: An open-access experimental dataset for arrays of wave energy conversion systems

SWELL: An open-access experimental dataset for arrays of wave energy conversion systems

Article *in* Renewable Energy · May 2023

DOI: 10.1016/j.renene.2023.05.069

6 authors, including:

Nicolás Faedo
Politecnico di Torino
80 PUBLICATIONS **874** CITATIONS
SEE PROFILE

Yerai Peña Sanchez
Universidad del País Vasco / Euskal Herriko Unibertsitatea
38 PUBLICATIONS **379** CITATIONS
SEE PROFILE

Edoardo Pasta
Politecnico di Torino
23 PUBLICATIONS **130** CITATIONS
SEE PROFILE

Guglielmo Papini
Politecnico di Torino
7 PUBLICATIONS **17** CITATIONS
SEE PROFILE

- Link to SWELL database: https://data.mendeley.com/datasets/n34wcksmts

SWELL: An open-access experimental dataset for arrays of wave energy conversion systems

Nicolás Faedo[a,*], Yerai Peña-Sanchez[b], Edoardo Pasta[a], Guglielmo Papini[a], Facundo D. Mosquera[c] and Francesco Ferri[d]

[a]Marine Offshore Renewable Energy Lab, Department of Mechanical and Aerospace Engineering, Politecnico di Torino, Turin, Italy
[b]Department of Mathematics, University of the Basque Country, Bilbao, Spain
[c]Instituto de Investigaciones en Electrónica, Control y Procesamiento de Señales, Universidad Nacional de La Plata, Buenos Aires, Argentina
[c]Department of the Built Environment, Aalborg University, Aalborg, Denmark

ARTICLE INFO

Keywords:
Wave energy
Wave energy converters
Array
Farm
Model validation
Data-based modelling

ABSTRACT

Achieving large-scale commercial exploitation of ocean *wave energy* inherently encompasses the design and deployment of arrays of wave energy converters (WECs), in an effort to reduce the associated levelised cost of energy. In this context, understanding the interactions between devices in a controlled WEC array is hence essential to achieve optimal layout configurations, as well as to provide guidance on the area required for array installation, reliability, life-time, and overall cost of the farm. Successful achievement of these vital objectives for the wave energy industry has been constantly aided by the use of appropriate *numerical models*. Regardless of the specific modelling approach adopted, model *reliability* is always a major concern: Numerical models need to able be to represent reality to be useful in supporting the different stages of development, hence providing significant results for decision making. To test reliability of a model, experimental results are an invaluable asset for validation.

Recognising the striking absence of real-world data concerning arrays of WEC systems, and its inherent value for model validation and data-based modelling purposes, we present, in this paper, an experimental campaign fully conducted with the sole objective of generating and providing an open-access dataset on WEC farms: *SWELL* (Standardised Wave Energy converter array Learning Library). The generated dataset, included alongside this manuscript, comprises an approximate total of ∼3000 variables and more than $\sim 10^8$ datapoints, for up to 5 devices in 9 diverse WEC array layouts with different levels of interaction, and 19 carefully selected operating conditions. Four different categories of tests are considered, providing measures of key variables required for model validation and data-based modelling tasks. As such, SWELL provides a crucial resource to achieve confidence in numerical modelling, helping towards creating reliable tools for decision making in the WEC field, hence effectively supporting the pathway towards effective commercialisation of ocean wave energy.

1. Introduction

The global energy demand has increased drastically over the course of both 20th and 21st centuries, continuously raising major concerns on the issue of future energy provision, with current predictions of an increase of nearly 50% between 2018 and 2050 [1]. With a (fortunately) growing awareness of the social and environmental challenges posed by fossil energy, and pressure to honour emission limits in the pathway towards a low-carbon energy society, a great deal of attention has turned to the effective and efficient use of renewable sources, in an effort to secure future energy needs [2, 3, 4, 5].

The potential of ocean renewable energies, to provide a major support in this quest, is already well-recognised across the globe, generating significant interest from governments and public entities, developers, and investors, all keen to provide assistance in effectively exploiting the many advantages of this renewable source. In particular, within the field of ocean renewables, the vast energy potential from ocean waves, *i.e. wave energy*, is, to date, largely untapped. With an estimation of an exploitable power resource of 30.000 [TWh/year] [6, 7, 8], wave energy can effectively provide a substantial contribution to the energy mix, being of a higher density than *e.g.* solar and wind power [9], consistently available (up to 90% of the time) [10], and highly predictable [11], with a negligible impact on the ocean environment when harvested properly [12, 13].

nicolas.faedo@polito.it (N. Faedo)
ORCID(s):

Although early efforts towards wave energy extraction date back to the 19th century (see *e.g.* [14]), availability of commercial harvesters remains elusive [15]. This can be attributed to a number of factors, including the rather diverse stochastic nature of the wave resource as a function of the location in the globe, survivability requirements in what can be considered a highly hostile environment, and a consequent lack of technology convergence towards an optimal wave energy converter (WEC) design/concept. This almost immediately translates to a higher levelised cost of energy (LCoE) with respect to sister renewables [15, 16], hindering effective and wide-spread commercialisation of WEC systems.

As it is well-established within the field, reducing the associated LCoE, and hence achieving large-scale commercial exploitation of wave energy, inherently encompasses two fundamental stepping stones. The first key enabler is linked to the use and development of appropriate control system technology, able to maximise the energy extracted by the WEC systems from the wave resource, while observing the underlying physical limitations characterising the device [17, 18]. Briefly summarising, the control problem for WEC systems consists in appropriate (and autonomous) manipulation of the force/torque exerted by the power take-off (PTO) system acting on the converter, in such a way that the energy conversion output is maximised, according to the current wave climate. Multipliers characterising the increase in energy absorption performance by means of appropriate control have been reported to be in the range of 2 to 4 (see *e.g.* [19, 20, 21]), with a degree of performance enhancement which ultimately depends on the particular nature of the WEC device and associated PTO system, and the specific control algorithm implemented [22].

The second key enabler to lower the LCoE, together with suitable control technology, is the deployment of WEC systems in array configurations (also often referred to as 'parks' or 'farms'), in an effort to reduce the associated costs (per device) of installation, operation, and maintenance, and ultimately to meet the required demands of installed capacity [23, 24, 25, 26]. Such arrays involve the deployment from a few to hundreds of WEC systems in a common area, arranged systematically according to a given layout configuration, typically designed in terms of row/column-like arrangements. In this context, a deep and detailed knowledge of the behaviour of WEC arrays is, hence, of paramount importance to achieve efficient farm configurations.

In particular, understanding the interaction effects between devices in a controlled WEC array is essential to achieve optimal layout configurations, as well as to provide insight on the effective area required for installation, reliability, life-time, and overall cost of the farm. As a matter of fact, WEC interactions can affect the overall performance of the array, having either positive or negative effects on the power absorption capabilities of neighbouring devices (see *e.g.* [27]) and, ultimately, on the associated LCoE [28]. Furthermore, given their capabilities of altering the surrounding wave field, it is equally important to measure the environmental impact that a given array can generate on proximal and distal wave climates [29, 30]. Successful achievement of these vital objectives for the wave energy industry has been constantly and consistently aided by the use of appropriate *numerical* (also referred to as '*mathematical*') *models*.

Mathematical models are of immeasurable value towards achieving commercialisation of WEC systems (and, in fact, absolutely crucial for virtually every branch of science), having the capabilities of giving insight and understanding on the behaviour of WECs in a set of pre-defined operating conditions. With a model in hand, one can predict the impact of a variety of design choices (*e.g.* number and inter-distance between devices, effective layout configuration, mid- and far-field effects, power take-off (PTO) system ratings, among others), being able to provide systematic information on how to manipulate, control, and optimise a given WEC array system outside the boundaries of physical reality, so as to achieve, as close as the application permits, a desired set of performance specifications. In essence, the enormous potential of mathematical models in wave energy can be attributed to the fact that these can be simulated in hypothetical situations and environments, subject to operating conditions that can be dangerous in reality, and without incurring in high costs before a process has been optimised accordingly. In fact, the latter has overseen the fall of a significant number of WEC companies, often not following a systematic development protocol supported by the use of appropriate numerical models, due to the high costs associated with full-scale device prototype construction, testing, commissioning, and de-commissioning.

Available standardised development protocols for WEC systems [25, 26, 31], often based on the well-known Technology Readiness Level (TRL) scale, unanimously agree on the use of numerical models to support the pathway towards commercialisation, starting from early stages (TRL 1-2), all the way up to full-scale WEC farm development, with different suggested (increasing) degrees of model fidelity. As such, a significant effort has been made by the research community towards comprehensive modelling of WEC farms, covering the full spectrum from low- to high-fidelity numerical simulation (see *e.g.* [29, 32, 33]). The low-fidelity end of the spectrum is well-populated, mostly by techniques based on so-called potential flow theory [32, 34], where linear assumptions are virtually always adopted. While indeed on the low-fidelity side, these models are extremely popular due to their representational and

computational convenience, being ideal for *e.g.* preliminary performance assessment, and a vast variety of control-oriented studies [18, 22]. Examples of this type of modelling approach for WEC arrays include [35, 36, 37, 38]. On the contrary, the high-fidelity end of the WEC array modelling spectrum often considers sophisticated numerical techniques, such as those based on Computational Fluid Dynamics (CFD), aiming at describing highly complex (nonlinear) phenomena, at the (potentially large) expense of computational power. Examples of modelling techniques belonging to this end of this spectrum are [39, 40, 41]. We further note that recent efforts have been done within the community towards the release of open-source design tools for WEC arrays, particularly within the European project DTOcean+ [42], which tackles development of numerical tools for structured innovation, stage-gating, and evaluation of wave farms.

Regardless of the specific technique/type of modelling approach considered, *model reliability* is always a major concern. In other words, numerical models need to be able to effectively represent reality to be useful in supporting the different stages of development, hence providing significant results for decision making [25, 26]. In this context, to test the reliability of a model, experimental results are an invaluable asset for *validation*. Furthermore, beyond the world of model validation, the availability of experimental data opens up the possibility to *data-based modelling* of WEC systems, where real-world information is directly fed into the modelling process, very much in the spirit of system identification [21, 43]. In spite of the significant value that such crucial information can have in supporting the pathway towards WEC commercialisation, publicly available datasets for WEC array experiments are incredibly scarse (if not inexistent), ostensibly due to the underpinning cost for small-scale prototype construction and instrumentation, and overall testing complexity. As a matter of fact, the number of real-world testing experiments on farm prototypes is reduced in itself (see *e.g.* the recent review paper [44]), let alone the data available for public use.

A number of well-established studies, effectively providing numerical datasets and benchmark cases for a single (stand-alone) WEC device, do exist within the state-of-the-art, and have been adopted with a great deal of success - see *e.g.* [45] and [46]. As a matter of fact, recent efforts have been done within the community towards effective and open sharing of full scale testing experience, with large projects such as *e.g.* OPERA [47], offering two years of open-sea data of both a floating WEC and a shoreline wave power plant. Nonetheless, availability of experimental datasets for the case of WEC arrays still remains elusive: to the best of the authors' knowledge, a single study [48] has been performed in the literature with the actual aim of providing an open-access dataset[1] on WEC farms for the development community. We note, although, that most of the effort in [48] has been only allocated in characterising the resulting (modified) wave field, for diverse WEC array configurations, disregarding a number of key variables required for validation and data-based model generation (such as *e.g.* effective wave force in the conversion degree-of-freedom (DoF)), limiting the scope of application of the generated experimental data to a subset of the modelling community. Furthermore, the devices in [48] have been tested without an actual PTO system, and a simple mechanical damping has been fashioned for each prototype, to emulate a (passive - see Section 4.4) control action. Finally, note that, as per the discussion provided at the beginning of this section, WEC systems require active control to maximise energy absorption, so validation of farm models under controlled conditions is of absolute importance for layout optimisation and overall performance assessment of a given configuration. We further clarify that the difference between controlled and uncontrolled behaviour can be substantial, with the former presenting larger device motion (and hence wave field interference), due to the action of the energy-maximising controller, which often enlarges the WEC operational space to maximise power absorption [22]. This fact, which can initially seem to be harmless within model validation/data-based modelling procedures, triggers a number of nonlinear effects that are not necessarily captured by models based on linear potential theory, hence potentially invalidating a family of models which would otherwise be considered validated in uncontrolled conditions [50].

Recognising the striking absence of real-world data concerning arrays of WEC systems, and its inherent value for model validation and data-based modelling purposes, we present, in this paper, an experimental campaign fully conducted with the sole objective of generating and providing an open-access dataset on WEC farms for any potential stakeholder, both within the academic, and industrial wave energy communities. The generated dataset, from now on termed *SWELL* (Standardised Wave Energy converter array Learning Library), included alongside this manuscript, is constructed on the basis of four different main tests, and comprises an approximate total of ∼3000 variables and more than $\sim 10^8$ datapoints, for up to 5 devices in 9 diverse WEC array layouts with different levels of interaction, and 19 carefully selected operating conditions (featuring regular, bimodal, irregular, and white noise sea states). In particular, as specifically discussed within Section 4, both the inherent synergy between the proposed standardised tests, and

[1] We do clarify that, at the moment of writing of this paper, the dataset of the experimental campaign conducted in [48] seems not to be open-access, but only available via specific request to the authors (see [49]).

corresponding layout configurations (chosen to maximise knowledge on the interaction between different devices in a diverse set of operating conditions - see Section 2.4), facilitate a well-posed learning procedure, able to characterise the main effects within WEC array systems under uncontrolled and controlled conditions, for different "levels" of interaction, recreated via the specific set of layouts considered. Within this experimental campaign, conducted in the wave tank facilities available at Aalborg University (Denmark), a small-scale (1:20) Wavestar-like [51] prototype is chosen as the baseline device, as depicted in Figures 1 and 3, effectively featuring an electric (direct drive) PTO system. We note that the choice of this system is not arbitrary, and is motivated by the large number of previous studies available on the (isolated) prototype [52, 53, 54, 55], being also featured as the baseline system for the so-called Wave Energy Control Competition (WEC^{3}OMP) [56]. As such, vast, transparent, and (virtually always) public information is readily available for this prototype within the WEC literature.

Four different categories of tests are considered to generate SWELL, providing measures of key variables required for model validation and data-based modelling tasks, including (but not limited to) free-surface elevation at different strategic points within the basin, force induced by the waves (*i.e.* wave excitation force), uncontrolled motion, and behaviour under the action of energy-maximising control, for each device, layout, and operating conditions considered. This is, to the best of our knowledge, the largest dataset characterising arrays of WEC systems available in the literature, including a wide variety of WEC layouts and realistic PTO effects (including energy-maximising control), tested in different scenarios following a consistent protocol, designed to suit the necessities associated with a vast number of modelling tasks. As such, the generated dataset SWELL provides a paramount resource to achieve confidence in numerical modelling, helping towards creating reliable tools for decision-making in the WEC field, hence effectively supporting the pathway towards commercialisation of ocean wave energy.

The remainder of this paper is organised as follows. Section 2 details the experimental setup considered, including wave tank facilities, baseline prototype and instrumentation, layout configurations, and PTO systems. Section 3 offers a detailed account of the sea states (operating conditions) considered, and the underlying criteria adopted for their choice within the experimental campaign. Section 4 provides an account of each test performed, including sample results to illustrate the dataset. Section 5 discusses the ordering and structure of SWELL, with specific reference to each of the variables present within the dataset, and their connection with the tests performed. Finally, Section 6 encompasses the main conclusions of this experimental campaign.

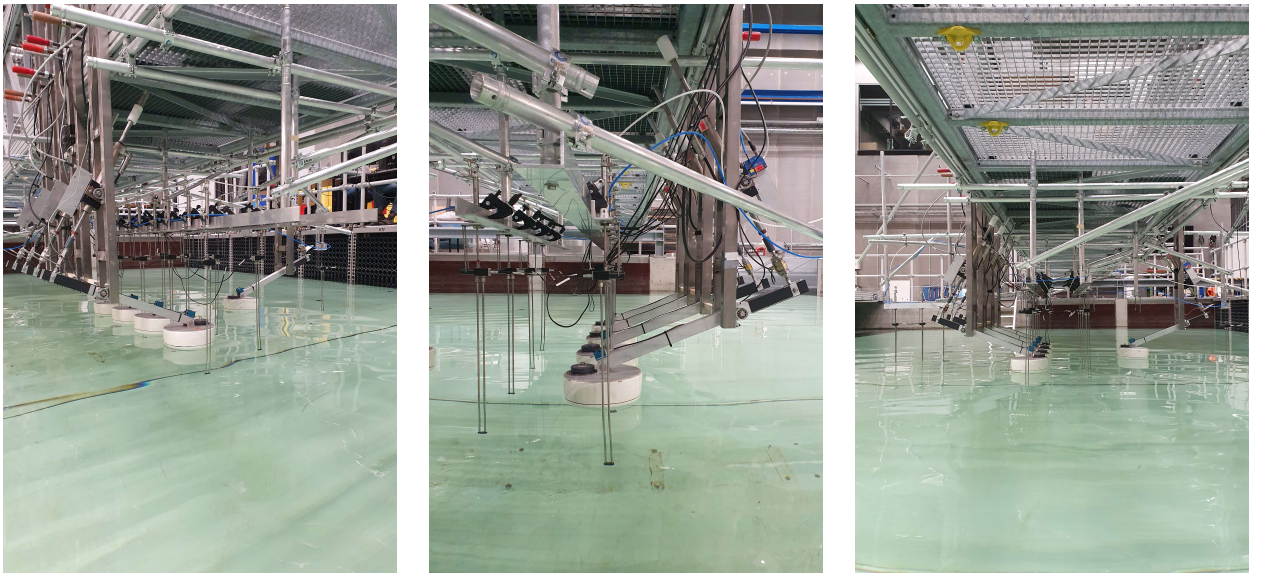

Figure 1: Photographs of the experimental setup designed for the WEC array experimental campaign, from different angles.

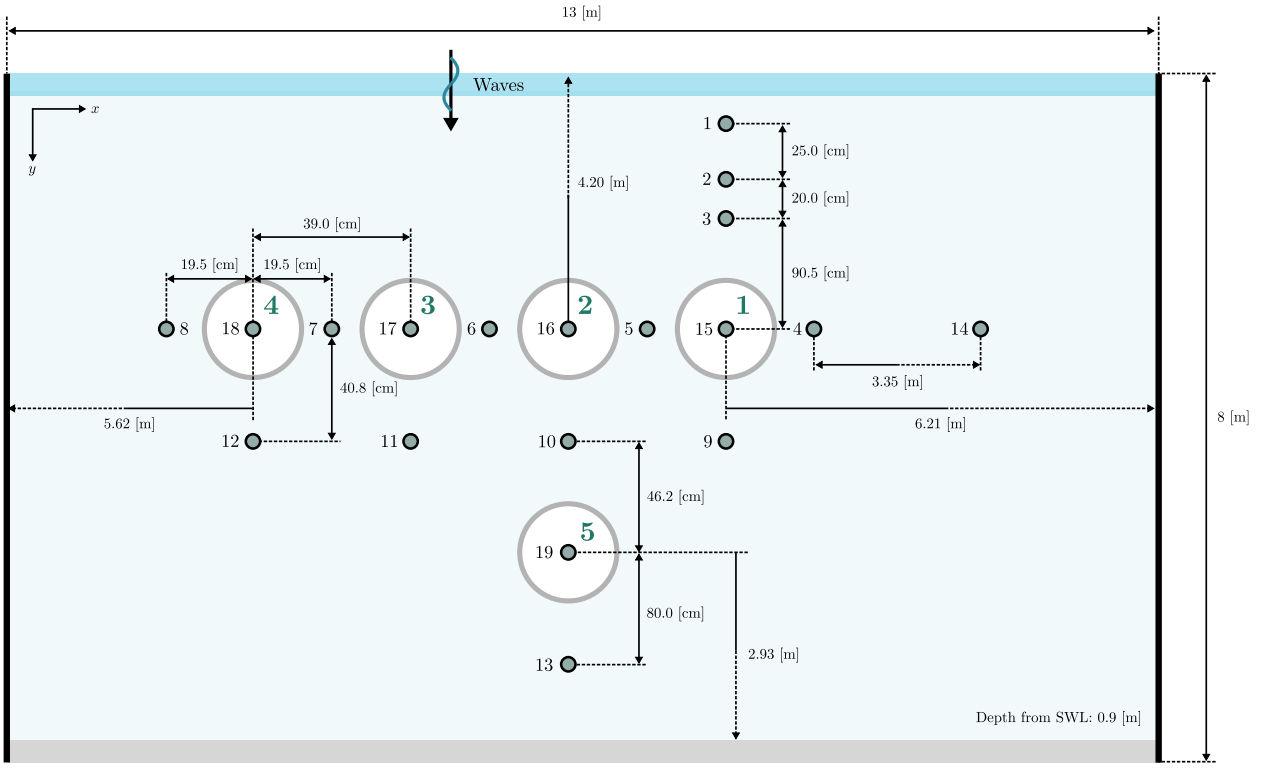

Figure 2: Schematic representation of the wave basin at the Ocean and Coastal Engineering Laboratory, in Aalborg University. The schematic includes the position associated with each device within the tank, and the location of the wave gauges used for free-surface elevation acquisition (grey-numbered circles in Figure). The acronym SWL stands for still water level. Note that gauges 15, 16, 17, 18 and 19 are only present for Test 1 (see Section 4).

2. Experimental setup and layout design

This section is dedicated to provide a detailed description of the experimental setup considered, as presented in Figure 1, including the Aalborg University wave tank specifications, baseline WEC system, equipment associated with each device and characterisation of PTO systems, WEC and wave gauges disposition within the wave tank, and considered array layout specifications. For the latter, we provide explicit motivation for the choice of each layout considered, with emphasis on specific aspects which are fundamental within validation/data-based modelling activities.

2.1. Wave tank specifications

The wave tank facilities, used to fulfil the objectives of this experimental campaign and effective generation of SWELL, are those available at the Ocean and Coastal Engineering Laboratory in Aalborg University, Denmark. The dimensions associated with the basin are as described in the schematic presented[2] in Figure 2. In particular, the available facilities comprise a basin of 19.3 [m] × 14.6 [m] × 1.5 [m] (length × width × depth), with an active test area of 13 [m] × 8 [m] (length × width). The wave tank is equipped with a state-of-the-art long-stroke segmented wavemaker system (custom-made by VTI [57]) with active absorption, composed of 30 individually controlled wave paddles, capable of producing a large variety of sea state conditions with high accuracy. Within this study, the water depth within the tank has been fixed to 0.9 [m], while the wavemaker is set to generate long-crested waves, *i.e.* parallel with respect to (w.r.t.) the x-axis, and with a direction of 0° on the y-axis, as indicated within Figure 2. In addition to the active absorption capabilities provided by the wavemaker system, the basin is equipped with passive wave absorption elements, built in stainless steel and hot galvanised stretch metal sheets. Finally, wave generation is performed using the in-house designed software AwaSys [58], which provides the wavemaker with an associated paddle movement reference for each tested wave, for effective wave realisation within the tank.

[2]Note that Figure 2 simply represents a schematic representation of the setup, and objects are not in-scale with respect to the tank dimensions.

2.2. Prototype WEC and acquisition system

The baseline WEC system, chosen for this array experimental campaign, is a 1:20 scale of the Wavestar wave energy conversion system [51]. The single unit of this prototype, which can be appreciated in Figure 3, essentially comprises a floater mechanically hinged to an out-of-the-water fixed reference point (point **A** in Figure 3). At the equilibrium position, the floater arm stands at approx. 30° w.r.t. the still water level (SWL). Note that the WEC is free to move in a single DoF. The main set of parameters associated with the single baseline prototype can be found in Table 1. The PTO (actuator) system is an electrical, direct-drive, linear motor (*LinMot Series P01-37 x 240F*), sitting on the upper structural joint composing the device (see Figure 3). The corresponding drive is a *LinMot E1200*, with a force rating up to ±200 [N].

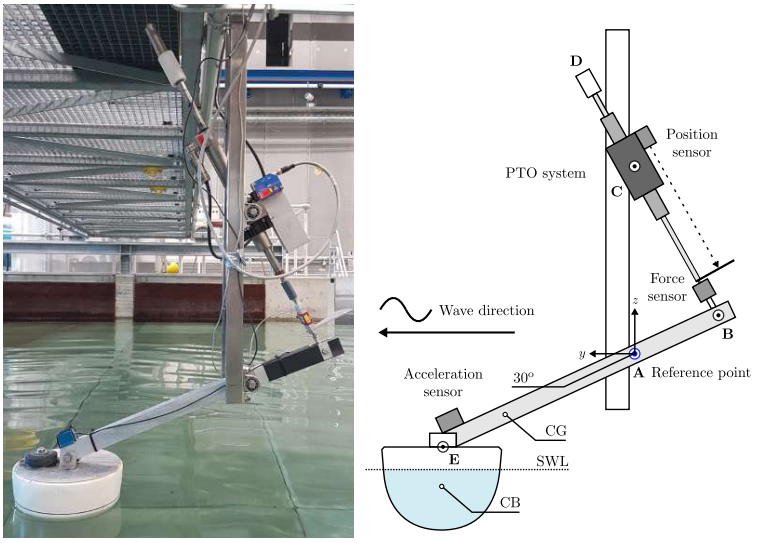

Figure 3: Photo of the baseline Wavestar prototype unit for the WEC array experimental campaign (left) and associated schematic representation (right). The acronym SWL stands for still water level.

Although translational displacement (associated with the PTO system) can be directly obtained as an output of the PTO driver, it is also measured via a dedicated laser position sensor (*MicroEpsilon ILD-1402-600*) for redundancy (see Figure 3), while the total force exerted on the PTO axis is measured by means of a *S-beam Futek LSB302* load cell. The system is equipped with a dual-axis accelerometer (*Analog Devices ADXL203*) sitting on top of the prototype floater, which, together with the translational motion measurements, is explicitly used to derive measures of rotational motion (*i.e.* angular displacement and velocity) about the fixed reference point A (see the schematic in Figure 3).

The data acquisition flow adopted is shown in Figure 4. The target PC is a Speedgoat Real-time Target Machine [59], which includes all the corresponding modules to handle input/output (I/O) variables, connected via a standard Ethernet to the host PC, transferring data using a user datagram protocol (UDP). Acquisition is consistently performed at a sampling rate of 200 [Hz], for all the acquired variables within the totality of the experimental campaign.

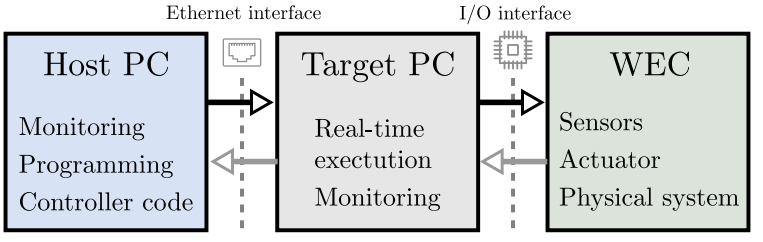

Figure 4: Schematic illustration of used sofware and hardware architecture.

Table 1
Main WEC parameters.

Parameter	Value (including units)
Floater mass	4 [kg]
Mass moment of inertia w.r.t. **A**	1 [kg m^2]
Floater draft	0.110 [m]
Floater diameter at SWL	0.256 [m]
Equilibrium position w.r.t. point **A** $\theta^0_{\mathbf{A}}$	0.523 [rad]
Distance points **A**-**C** $L_{\mathbf{AC}}$	0.412 [m]
Distance points **C**-**B** $L_{\mathbf{CB}}$ (in eq.)	0.381 [m]
Distance points **A**-**B** $L_{\mathbf{AB}}$	0.200 [m]
Distance points **A**-**E** $L_{\mathbf{AE}}$	0.484 [m]
Distance points **A**-**E** in y	0.437 [m]
Distance points **A**-**E** in z	0.210 [m]
Centre of gravity in y	0.415 [m]
Centre of gravity in z	-0.206 [m]
Centre of buoyancy in y	0.437 [m]
Centre of buoyancy in z	-0.321 [m]
Arm mass	1.157 [kg]
Arm moment of inertia w.r.t. **A**	0.060 [kg m^2]

From now on, and, in particular, throughout Section 4, we use the following convention w.r.t. the WEC prototype main variables, all of which (either by direct measurement or reconstruction/estimation) are effectively part of the associated open-access dataset SWELL[3]:

(M) Measured variables:

- z_{PTO}: Linear displacement (in [m]) of the PTO motor. This can be measured either via the incorporated driver sensor, or the laser sensor on top of the PTO axis.
- $\ddot{z}_{\mathbf{E}}$: Linear acceleration (in [m/s^2]) of the WEC floater at point **E**. This can be measured by virtue of the accelerometer on top of the floater.
- $f_{\mathbf{B}}$: Force (in [N]) at point **B**. This can be measured directly by the load cell sitting on the PTO axis.

(E) Reconstructed/estimated variables:

- $\tau_{\mathbf{A}}$: Torque (in [Nm]) w.r.t. point **A**.
- $\theta_{\mathbf{A}}$: Angular displacement (in [rad]) of the WEC prototype w.r.t. point **A**.
- $\dot{\theta}_{\mathbf{A}}$: Angular velocity (in [rad/s]) of the WEC prototype w.r.t. point **A**.
- $\ddot{\theta}_{\mathbf{A}}$: Angular acceleration (in [rad/s^2]) of the WEC prototype w.r.t. point **A**.

In particular, $\tau_{\mathbf{A}}$, $\theta_{\mathbf{A}}$, and $\ddot{\theta}_{\mathbf{A}}$ can be reconstructed using the set of measured variables listed above in (M), *i.e.*

$$\begin{aligned}
\tau_{\mathbf{A}} &= f_{\mathbf{B}} \cos\left(\sin^{-1}\left(\frac{L_{\mathbf{AC}}^2 - L_{\mathbf{AB}}^2 - \left(L_{\mathbf{CB}} + z_{\text{PTO}}\right)^2}{-2L_{\mathbf{AB}}^2\left(L_{\mathbf{BC}} + z_{\text{PTO}}\right)}\right)\right) L_{\mathbf{AB}}, \\
\theta_{\mathbf{A}} &= \theta^0_{\mathbf{A}} - \sin^{-1}\left(\frac{\left(L_{\mathbf{CB}} + z_{\text{PTO}}\right)^2 - L_{\mathbf{AC}}^2 - L_{\mathbf{AB}}^2}{-2L_{\mathbf{AC}}L_{\mathbf{AB}}}\right), \\
\ddot{\theta}_{\mathbf{A}} &= \frac{\ddot{z}_{\mathbf{E}}}{L_{\mathbf{AE}}}.
\end{aligned} \tag{1}$$

Table 2 offers a summary of the considered sensor/actuation equipment, and their corresponding measurement capabilities/uncertainty (as per each associated manufacturer datasheet), for each of the variables listed in (M). The

[3]From now on, the dependence on t is dropped when clear from the context.

Table 2
Instrumentation and corresponding measurement capabilities.

Sensor/actuator	ID	Measurement variable	Uncertainty
Linear motor	LinMot Series P01-37 x 240F	Linear position z_{PTO}	± 0.05 [mm]
Laser position sensor	MicroEpsilon ILD-1402-600	Linear position z_{PTO}	± 80 [μm]
Load cell	S-beam Futek LSB302	Force at point **B** $f_{\mathbf{B}}$	± 0.125 [N]
Accelerometer	Analog Devices ADXL203	Linear floater acceleration at point **E** $\ddot{z}_{\mathbf{E}}$	± 0.01 [m/s^2]
Wave gauges	VTI WG-8CH	Wave elevation at 19 points in the basin	± 0.04 [mm]

only variable in (E) which cannot be directly computed via the measured quantities in (M) is the velocity of the system w.r.t. point **A**, *i.e.* $\dot{\theta}_{\mathbf{A}}$, requiring effective estimation. To do this with the available measures, described in the paragraph immediately above, we employ standard methodologies for sensor fusion, and we leverage a Kalman Filtering (KF) technique (see *e.g.* [60]) to provide estimates of $\dot{\theta}_{\mathbf{A}}$ when needed.

2.3. Wave gauges and devices positioning

Measurements of free-surface elevation are obtained by using wave probes (WP), also often called wave gauges, of a resistive-type (*VTI WG-8CH*). In particular, 19 WPs have been considered within this experimental campaign, located at strategic points within the wave tank, as can be appreciated in Figure 2.

The set of WPs {1, 2, 3}, aligned w.r.t. the centre line of device 1 (D1), is placed in a column-like pattern, with different inter-distances between WP 1 - WP 2 and WP 2 - WP 3. WPs 4 to 8 are strategically placed in the middle position between each set of devices, allowing for an explicitly measure of *e.g.* radiated waves between bodies, whose intensity naturally depends on the specific layout considered (discussed within this section in the following paragraphs). WPs 9 to 13 are located behind (w.r.t. the wave generation direction) each of the devices considered, providing further information on the resulting wave field for each test and layout employed within this campaign. WPs 15 to 19, which are potentially among the most relevant set of probes, give information on the free-surface elevation at the centre position of each device involved. This is particularly useful for I/O modelling, including *e.g.* parametric structures for control/estimation purposes (see *e.g.* [21, 43]). Note that WPs 15 to 19 are only effectively present within the basin whenever the devices are not in place, *i.e.* for measuring free-surface elevation corresponding with each considered sea state without the presence of the WECs in the tank (see Test 1 in Section 4). Finally, WP 14 is used as a 'control' probe for all the tests performed, and is placed in an area away from the active device zone.

Regarding device positioning, 5 prototypes (D1 to D5) are considered and placed within the wave basin for this WEC array experimental campaign, each mounted on a gantry by means of a supporting structure (see Figure 1). D1 to D4 are placed in a row-like formation, with a distance of 39 [cm] from centre to centre of adjacent devices. Note that this corresponds to approximately 1.5 times the diameter of the prototype floater (see Table 1), resulting in an inter-device distance (floater edge-to-edge) of approximately 1 radius, *i.e.* 13 [cm]. Each device can be lifted out of the basin manually, hence allowing for testing of different layout configurations by simply pulling a specific set of devices out of the water. Finally, we note that D5, which is mounted on the rear side of the gantry, is placed in a 'flipped' position w.r.t. devices D1 to D4 (see Figure 1). This specific placement has been pursued with the objective of providing a heterogeneous array configuration in an effort to enrich the results (and, hence, the associated dataset), *i.e.* the response of D5 will be naturally different from that of D1 to D4.

2.4. Array layout design

We consider 9 different layout configurations (L0 to L8) involving up to 5 different devices operating simultaneously within the basin, as schematically illustrated within Figure 5. The choice of these layouts is, naturally, not arbitrary, as detailed in the following. We first note that the testing set is comprised of two layouts with a single device (L0 and L8), three with two devices (L1 to L3), two with three prototypes (L4 and L5) and, finally, one layout with 4 and 5 WECs operating within the basin (L6 and L7, respectively).

L0, which, as discussed within Section 1, has been considered previously in the modelling/validation literature for this specific Wavestar prototype (see *e.g.* [53, 56, 61, 62]), is chosen as the baseline case, and is essentially comprised of a standard single device configuration. Given the mounting and positioning of D5 (see Section 2.3), L8 is considered to provide data to characterise, in a stand-alone fashion, the heterogeneous component among devices. L1 to L3 constitute the first set of tested layouts with more than a single WEC prototype. These layouts are designed with essentially the same formation, but with different inter-device distances. The underpinning design for L1 to L3 allows for a direct

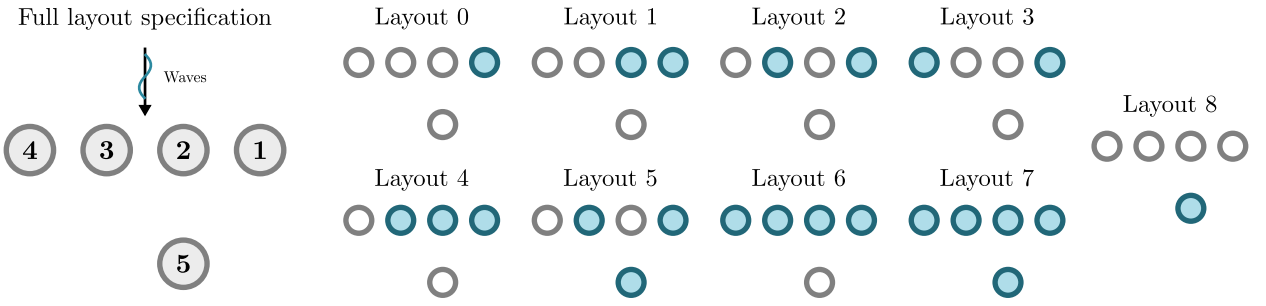

Figure 5: Full set of layouts considered within the WEC array experimental campaign presented in this study.

characterisation of the effect of interactions between devices as a function of the distance between bodies, which is fundamental to understand constructive/destructive effects within WEC array configurations (see *e.g.* [27, 63, 64, 65]). L4 and L5 incorporate a third device into the basin, and are designed as a natural 'extension' of L1 and L2. Note that, while L4 includes a device in-between D1 and D3 (*i.e.* in a row-like formation), L5 considers a triangle-like shape, incorporating D5 into the wave tank. Finally, L6 offers a four-device row formation, essentially comprised of all the devices used in L0 to L4, *i.e.* D1 to D4, while L7 represents the potentially most complex case from a modelling and configuration perspective, including all 5 devices, operating simultaneously within the basin.

2.5. Characterisation of PTO dynamics

Since the considered WEC prototype systems are, effectively, designed to represent a scaled version of the Wavestar wave energy converter, they incorporate an actual PTO actuator (linear motor - see Section 2.2) accordingly. These motors, which are able to exert a force along their axis, can essentially operate in two different modes, *i.e.* force and position control. In the case of the former, adopted within the presented experimental campaign, a target (reference) PTO force $u_{\text{PTO}}^{\text{ref}}$ (as in Figure 6) is sent to each associated driver which, via a dedicated proportional-integral-derivative (PID) controller, attempts to effectively tracking the requested force, providing a signal u_{PTO} to the WEC system. We emphasise, at this point, that there exists a clear distinction between the PTO driver controller, whose only objective is that of force reference tracking (as described immediately above), and what it is termed 'WEC controller' in Figure 6, which is in charge of providing a reference force to the PTO system so as to maximise energy extraction from the wave resource (see the discussion provided in Section 1). The latter is also considered explicitly within this experimental campaign, as detailed throughout Section 4.4.

Though the final objective of this paper is that of providing a dataset characterising real WEC array prototypes, *i.e.* in real-world conditions, we do appreciate that a large part of the WEC modelling community is focused on numerical representation and validation of the hydrodynamics pertaining to such devices in idealised conditions, *i.e.* without the incorporation of a (realistic) PTO system. With this in mind, we provide, within this section, both a discussion and experimental characterisation of these linear motors, and hence the overall PTO dynamics, for the benefit of the reader and potential users of SWELL.

With the exception of Tests 1 and 2 (as listed in Section 4), the linear motor is always required to operate in force control conditions. As such, we tune the parameters of the associated force (driver) controller to achieve a sufficiently large bandwidth, being able to effectively track any of the force signals required during the campaign, *i.e.* such that, ideally, $u_{\text{PTO}}^{\text{ref}} \approx u_{\text{PTO}}$ (see also Figure 6). In this way, we guarantee that the associated motor dynamics interfere as little as possible with those characterising the mechanical energy conversion process of the WEC system. Naturally, since we are dealing with real-world systems, the PID tuning procedure has to be achieved by accepting a suitable compromise between effective bandwidth and *e.g.* stability and noise amplification (the interested reader is referred to *e.g.* [66] for a detailed discussion). In other words, the linear motor cannot be controlled to be arbitrarily fast, as one would be able to do within idealised (simulation) conditions.

The driver PID tuning procedure has been performed in-situ, by using standard I/O tests and associated techniques (see *e.g.* [67]). The dataset includes an experimental characterisation of the I/O behaviour of each (driver-controlled) linear motor, obtained by means of chirp experiments (see *e.g.* [68]). In particular, a set of chirp driver reference force signals with amplitudes in the set $\{15, 17.5\}$ [N] and frequency content within 0.1 [rad/s] and 15 [rad/s] (which covers accordingly the frequency range characterising the WEC operating conditions - see Section 3) has been injected into

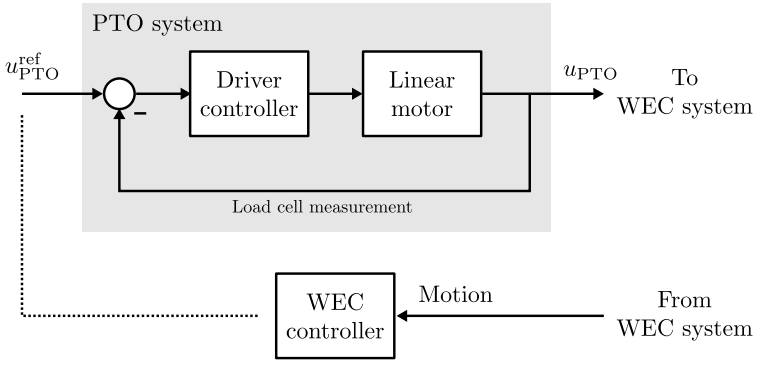

Figure 6: Schematic illustration of the PTO system and associated control architectures.

each individual PTO motor as $u^{\text{ref}}_{\text{PTO}}$, generating a set of corresponding force outputs u_{PTO}. By way of example, Figure 7 shows an I/O pair for a chirp test with a reference amplitude of 17.5 [N], applied to the linear PTO motor associated with D2.

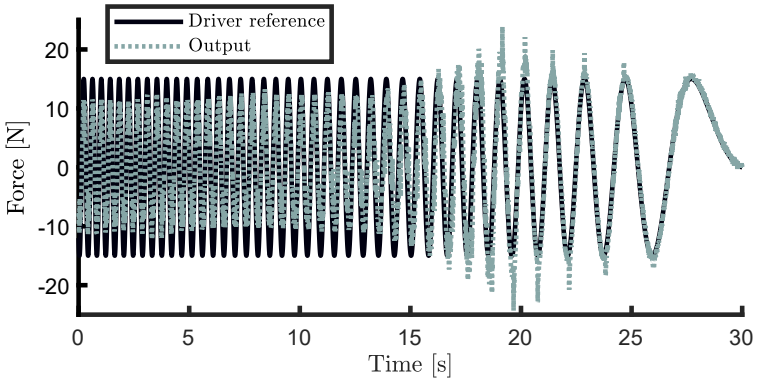

Figure 7: Example I/O pair for the PTO chirp tests provided as part of the dataset, executed on the motor associated with D2.

Another potentially relevant component, which is inevitably present in this type of PTO systems, are friction effects. In fact, the sharp 'peaks' that can be seen in the chirp test presented within Figure 7, are directly linked to such phenomena: the PTO motor 'sticks' to the axis at low speeds, presenting a typical dead-zone behaviour (see *e.g.* [69]). While these effects are effectively minimised by appropriate tuning of the driver internal controller, a PI structure is, clearly, not sufficient to fully counteract friction. Nonetheless, as discussed previously within this paragraph, friction effects become potentially relevant at very low speeds, which do not normally occur in operating conditions for the WEC device (especially when $u^{\text{ref}}_{\text{PTO}}$ is designed according to energy-maximising control conditions, where both displacement and velocity tend to be higher in order to maximise energy absorption - see Section 4.4).

Nonetheless, aiming to provide a dataset as comprehensive as possible, a characterisation of these friction effects is also included within SWELL (see Section 5), performed in terms of slow and fast motion tests for each PTO system associated with all five devices. These tests are executed by moving the floater (and hence the motor axis) manually, both at low and high speeds (see *e.g.* [44]). Exploiting motion and measured force, these tests incorporate, within the dataset, an experimental characterisation of both static and dynamic friction effects associated with each PTO actuator. By way of example, Figure 8 shows a time-snippet of such test performed on the PTO system of D2, where both slow and fast motions (and associated measured force on the motor axis) can be effectively appreciated.

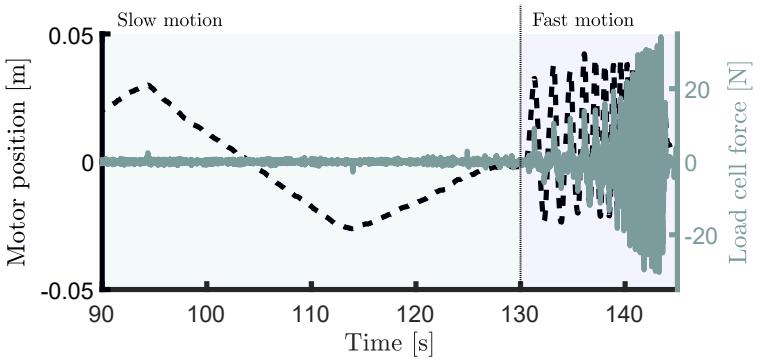

Figure 8: Example I/O pair for the friction tests provided as part of the dataset, executed on the motor associated with D2.

Table 3
Waves tested within the presented experimental campaign.

ID	Type	Period [s]	Height [m]	γ	#R	Length [s]
RSS1	Regular	0,8	0,05	-	1	60
RSS2	Regular	0,9	0,05	-	3	60
RSS3	Regular	1	0,05	-	1	60
RSS4	Regular	1,2	0,05	-	3	60
RSS5	Regular	1,5	0,05	-	1	60
BMSS	Bimodal	{0.9, 1.2}	Equal energy	-	1	60
ISS1	Irregular	1,412	0,063	3,3	2	300
ISS2	Irregular	1,836	0,104	3,3	2	300
ISS3	Irregular	0,988	0,0208	1	2	300
WNSS1	W. noise	[0.5, 10]	0,01	-	1	300
WNSS2	W. noise	[0.5, 10]	0,03	-	1	300
WNSS3	W. noise	[0.5, 10]	0,05	-	1	300
Total number of waves tested: 19						

3. Definition of sea states

This section provides a description of the sea states considered within the campaign, emphasising the underlying motivation for their choice, and potential use for different modelling/validation tasks. A total of 12 sea states are considered, with a different number of realisations (#R) depending on the specific operating condition. Four types of sea states are included within SWELL, as briefly listed below:

- *Regular sea state* (RSS): Waves generated with a monochromatic spectrum, *i.e.* deterministic, with one single component at a specific frequency.
- *Bimodal sea state* (BMSS): Waves generated with a bichromatic spectrum, *i.e.* deterministic, with two selected components in frequency.
- *Irregular sea state* (ISS): Waves generated in terms of a representative stochastic representation. In particular, JONSWAP spectra [70] are considered within this study, as further discussed within Section 3.3.
- *White noise sea state* (WNSS): Waves generated in terms of a constant spectral density in a pre-defined frequency range.

A detailed discussion on each type of sea state is provided below, while a summary of the operating conditions considered within this paper is offered within Table 3.

3.1. Regular sea states

Though regular waves can be limiting from a representational perspective, *i.e.* they emulate sea state conditions with a single frequency component, these can still be useful to achieve a number of modelling/validation objectives. First of all, having a single frequency component allows for 'decoupling' of a certain number of effects, which can be easily masked in the irregular wave case. For instance, nonlinearities tend to be more clear in regular-type of tests since, being the wave input composed of a single component, any nonlinear behaviour would generate a set of sub- or super-harmonics of such a frequency[4], clearly appreciated in system motion. Furthermore, regular waves also represent a useful tool for preliminary analysis of energy-maximising WEC controllers, being the designer able to verify a set of well-known optimality conditions almost straightforwardly (*e.g.* phase locking between wave excitation and WEC velocity [19, 72]). Finally, monochromatic waves are commonly used when modelling extreme wave conditions, and are hence useful for performing validation of *e.g.* stress models [73].

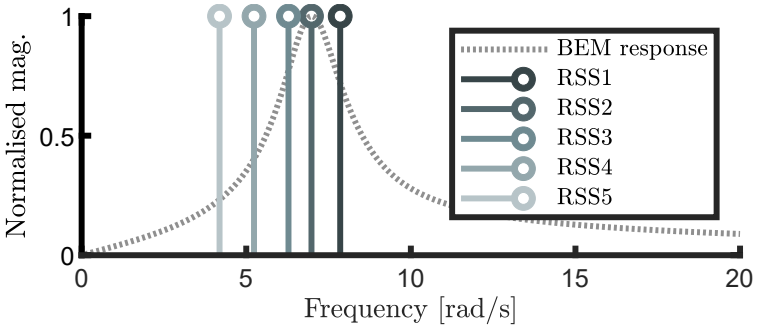

Figure 9: Theoretical spectra for the regular wave conditions used within this experimental study.

Within this study, and hence SWELL, five different regular wave conditions are considered (RSS1 to RSS5 - see Table 3), with frequency components selected strategically w.r.t. the device response, and a constant wave height. In particular, Figure 9 shows the theoretical spectrum associated with each RSS condition (solid lines), normalised w.r.t. that with the highest energy, for representational purposes. The dashed line in Figure 9 represents the magnitude associated with the torque-to-motion (*i.e.* input: wave excitation torque - output: floater angular velocity) frequency-response map for the baseline Wavestar prototype system described in Section 2.2, computed using a BEM solver[5]. Note that waves are chosen to cover the typical operational space for this system, including resonance (RSS2), low (RSS3, RSS4 and RSS5), and high (RSS1) frequency behaviour. In addition, note that different number of realisations #R has been considered, depending on the specific RSS. Though these sea states are effectively deterministic, the choice of generating more than a single realisation for a subset of these operating conditions is performed to equip the dataset SWELL with information on the capabilities of the wavemaker system to reproduce a given sea state in different runs. Finally, we note that a constant wave height has been chosen in order to provide analogous results for all (frequency) conditions. The specific choice of wave height has been done by considering any limitations associated with the wave generation system which, according to the period, can accurately generate waves within the basin up to a certain height limit.

3.2. Bimodal sea state

As discussed within Section 3.1, sea states composed of a finite number of components, although not realistic in practice, can be useful for identification of complex phenomena characterising WEC systems. Bimodal sea states represent a natural extension of the regular wave case, by incorporating an additional frequency component. These wave conditions which, in practice, are linked to a combination of wind- and swell-seas, can be used within the scope of modelling/system dynamics to *e.g.* infer measures of nonlinear behaviour of the system by quantifying the validity of the principle of superposition for these specific components [75], or even to provide an estimation of the class of functions characterising the nonlinearities of the WEC [71, 76]. Furthermore, while high-fidelity numerical wave tanks are virtually always able to generate regular waves with great precision, these is not necessarily the case for

[4]Presence of either sub- or super- harmonics intrinsically depends on the stability nature of the system (see *e.g.* [71]).

[5]The open-source BEM software NEMOH [74] has been used to compute the associated prototype frequency-response map.

polychromatic sea states [77, 78], so that bimodal sea states can represent a useful 'intermediate' case between regular and irregular conditions for numerical validation purposes.

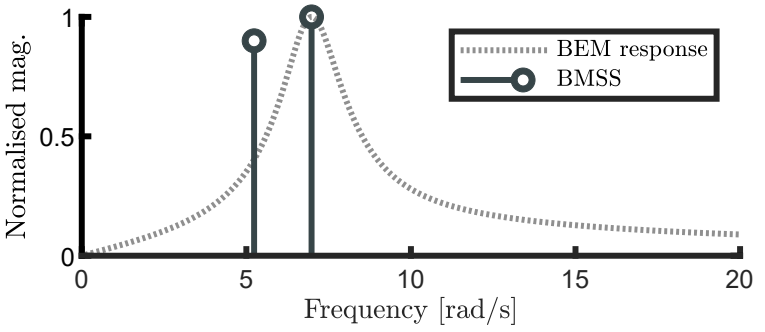

Figure 10: Theoretical spectra for the bimodal wave condition used within this experimental study.

Within this experimental campaign, we consider a single bimodal sea state (BMSS - see Table 3), with one frequency component placed at the resonance behaviour of the WEC prototype (equivalent to RSS2), and a low-frequency contribution (equivalent to RSS4). An equal energy method (see *e.g.* [79]) has been employed to characterise the associated theoretical spectrum, which can be appreciated within Figure 10 (normalised w.r.t. the frequency placed at the system resonance).

3.3. Irregular sea states

As it is virtually always the case within the marine/ocean engineering community, realistic waves can be represented in terms of a set of stochastic descriptions, with an associated (dense) spectrum (see *e.g.* [80]). While different models can be used to characterise ocean waves, a particularly well-used representation is that provided by the so-called JONSWAP spectrum [70], describing wind-generated seas with fetch limitations. Within such a stochastic description, three main parameters can be identified, *i.e.* significant wave height H_s, peak wave period T_p, and peak-enhancement factor γ.

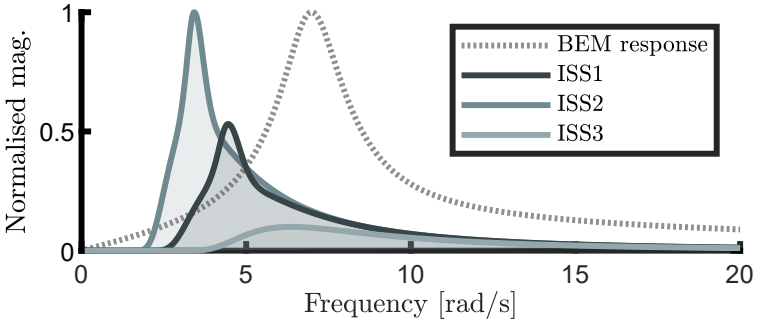

Figure 11: Theoretical spectra for the irregular wave conditions used within this experimental study.

Three irregular sea states (ISS1 to ISS3) are considered within this experimental campaign, as described within Table 3. The parameters for these conditions have been directly adopted from the benchmark control case established by the WEC^{3}OMP [56], and aim to represent diverse operating sea states for both uncontrolled, and controlled device motion conditions. The theoretical spectra (normalised w.r.t. ISS2) associated with these sea states can be appreciated in Figure 11. Two narrow-banded conditions (ISS1 and ISS2) are considered, with different peak periods and associated significant wave heights. Finally, ISS3 represents a broad-banded operating case, with significant energy content covering low-, resonance, and high-frequency components. Note that two different realisations are considered for each ISS, so as to provide the dataset with diverse (time-domain) representations for each operating condition.

3.4. White noise waves

While irregular sea states, as described within Section 3.3, can effectively represent realistic wave conditions, these might not be fully useful for *e.g.* control-oriented modelling/validation. In particular, since WEC systems have to operate in potentially (very) different sea states, having diverse spectral content and characterisation, modelling/validation of *e.g.* WEC controllers for a broad range of operating scenarios can become difficult (and time-consuming - especially in *e.g.* CFD-based models) with a limited number of irregular sea states tests. Aiming to resolve this issue, we employ, within this experimental campaign, sea states described in terms of white noise spectra, *i.e.* with a constant spectral density function in a sufficiently large (yet banded) frequency range. The latter has to be large enough to thoroughly cover the typical WEC operating conditions, hence guaranteeing representativity of the associated dataset for a large number of operating scenarios.

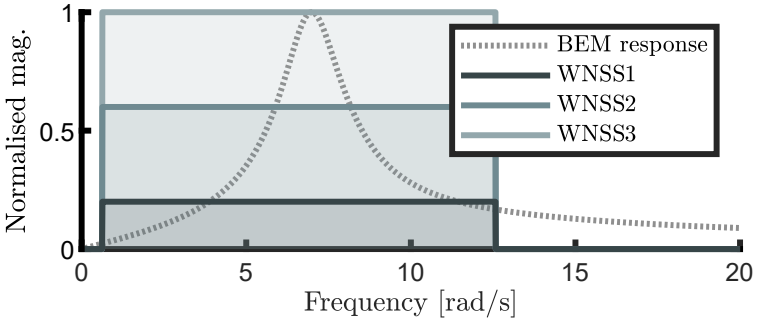

Figure 12: Theoretical spectra for the white noise wave conditions used within this experimental study.

In particular, three different white noise sea states (WNSS1 to WNSS3) are considered within this experimental campaign, as described within Table 3, and presented in Figure 12. While, as can be appreciated from Figure 12, the frequency range, which effectively contains the main dynamics of the baseline WEC prototype, remains constant for WNSS1, WNSS2 and WNSS3, their energy increases progressively. This is performed to provide information on how a higher energy content (which effectively translates to larger free-surface elevation points in time) has an effect on the system response, hence supplying data on any relevant nonlinear behaviour affecting the WEC prototypes according to each tested layout.

4. Tests design and sample results

Having described the baseline prototype and array layouts in Section 2, and the considered sea states for experimental generation of SWELL within the Aalborg University wave tank in Section 3, we proceed to describe in detail the specific set of tests considered, and their associated nature and synergy. Four different tests have been designed, in which either all, or a subset of the considered sea states and WEC array layouts (see Table 4) are involved:

Test 1 *Free-surface elevation*: Test designed to provide the wave elevation (time-domain) signal for each sea state and realisation considered within this experimental campaign, at the probe locations described in Figure 2. Note that, as further detailed within Section 4.1, this test is effectively independent on the layout definitions provided in Section 2.4.

Test 2 *Wave excitation*: Test designed to provide the wave excitation force/torque associated with each generated free-surface elevation, for each sea state and realisation considered within this experimental campaign, and each WEC array layout specified within Section 2.4.

Test 3 *Uncontrolled device motion*: Test designed to provide *uncontrolled* WEC device motion (displacement, velocity and acceleration) associated with each generated free-surface elevation, for each sea state and realisation considered within this experimental campaign, and each WEC array layout specified within Section 2.4.

Test 4 *Controlled device motion*: Test designed to provide *controlled* WEC device motion (displacement, velocity and acceleration) associated with each generated free-surface elevation, for each sea state and realisation considered within this experimental campaign, and each WEC array layout specified within Section 2.4.

Table 4
Executed tests as a function of both sea states and WEC array layouts considered. The symbol ● indicates that the tests have been performed on L0 to L8, while those with ○ have been considered on L0 to L5.

	Test 1	Test 2	Test 3	Test 4
R1	●	●	●	-
R2	●	●	●	-
R3	●	●	●	-
R4	●	●	●	-
R5	●	●	●	-
BM	●	●	●	-
ISS1-1	●	●	●	○
ISS1-2	●	●	●	-
ISS2-1	●	●	●	○
ISS2-2	●	●	●	-
ISS3-1	●	●	●	○
ISS3-2	●	●	●	-
WNSS1	●	●	●	-
WNSS2	●	●	●	-
WNSS3	●	●	●	-

Each test is described in detail in a specific section (Sections 4.1 to 4.4), following this paragraph. Specific emphasis in the connection and synergy between Tests 1, 2, 3 and 4 is made within Section 4.5. We further clarify that the objective of this section is not that of providing a comprehensive analysis of the dataset provided within this paper, but to introduce the nature of the tests and a set of sample results, used to illustrate their execution.

4.1. Test 1: Free-surface elevation

This test has the final objective of providing a measure, within SWELL, of the time-series associated with free-surface elevation for each of the sea states (and realisations) listed in Section 3. These measures are taken at diverse points (in space) within the wave tank, according to the description provided within Section 2.3. Note that, for this particular test, no device is present within the tank, so that the wave probes WP 15, 16, 17, 18 and 19 effectively measure free-surface elevation at the centre point of each WEC system when in operating conditions (see Figure 2).

To illustrate the effective measurement of free-surface elevation, Figure 13 shows the time-traces associated with RSS1 to RSS5 and that of BMSS, as measured by WP 1, and the magnitude associated to their respective fast Fourier transform (FTT). Note that the wavemaker is effectively able to produce these waves with high precision, having their energetic content effectively concentrated in either a single component (RSS - first four from the top) or in two separate frequencies (BMSS - bottom), coinciding well with their theoretical description (see Section 3). To further extend the example provided by Figure 13, Figure 14 illustrates measurements obtained by WP 1 for ISS1-1, ISS2-1, ISS3-1, and the three white noise wave conditions (WNSS1, WNSS2 and WNSS3). A good agreement with the theoretical spectrum can also be qualitatively appreciated from Figure 14, for all the analysed cases.

To demonstrate the repeatability of the wavemaker, Figure 15 shows a time-snippet (of approximately two wave periods) associated with the three realisations tested of RSS2 and RSS4, as measured by WP 1. A very good agreement can be appreciated between all separate wave generation experiments, showing the capabilities of the wavemaker to consistently generate the same wave in diverse frequency points.

We discuss one last issue within this section, which is that of wave probe alignment. As can be appreciated in Figure 2, a large set of probes has been placed in a row-like formation, so as to measure the wave elevation consistently in-between devices, and their centre points. By way of example, Figure 16 shows measurements of free-surface elevation for WP 15, 16, 17 and 18, placed at the central position of D1, D2, D3 and D4, respectively, for ISS1-1. As it can be appreciated, the measurements show a very good agreement, both in a point-to-point comparison (top), and w.r.t. their normalised correlation (bottom), using WP 15 as the 'target' signal (*i.e.* computed w.r.t. WP 15). Note that the latter shows a maximum correlation point at ≈ 0 [s] (in lag), effectively validating the placement of the probes within the wave tank.

Nonetheless, though ideally the same signal, one can realise, from Figure 16 (top), that the measurements of WP 15, 16, 17 and 18 present slight differences between each other. This can be at least partially explained by any reflections

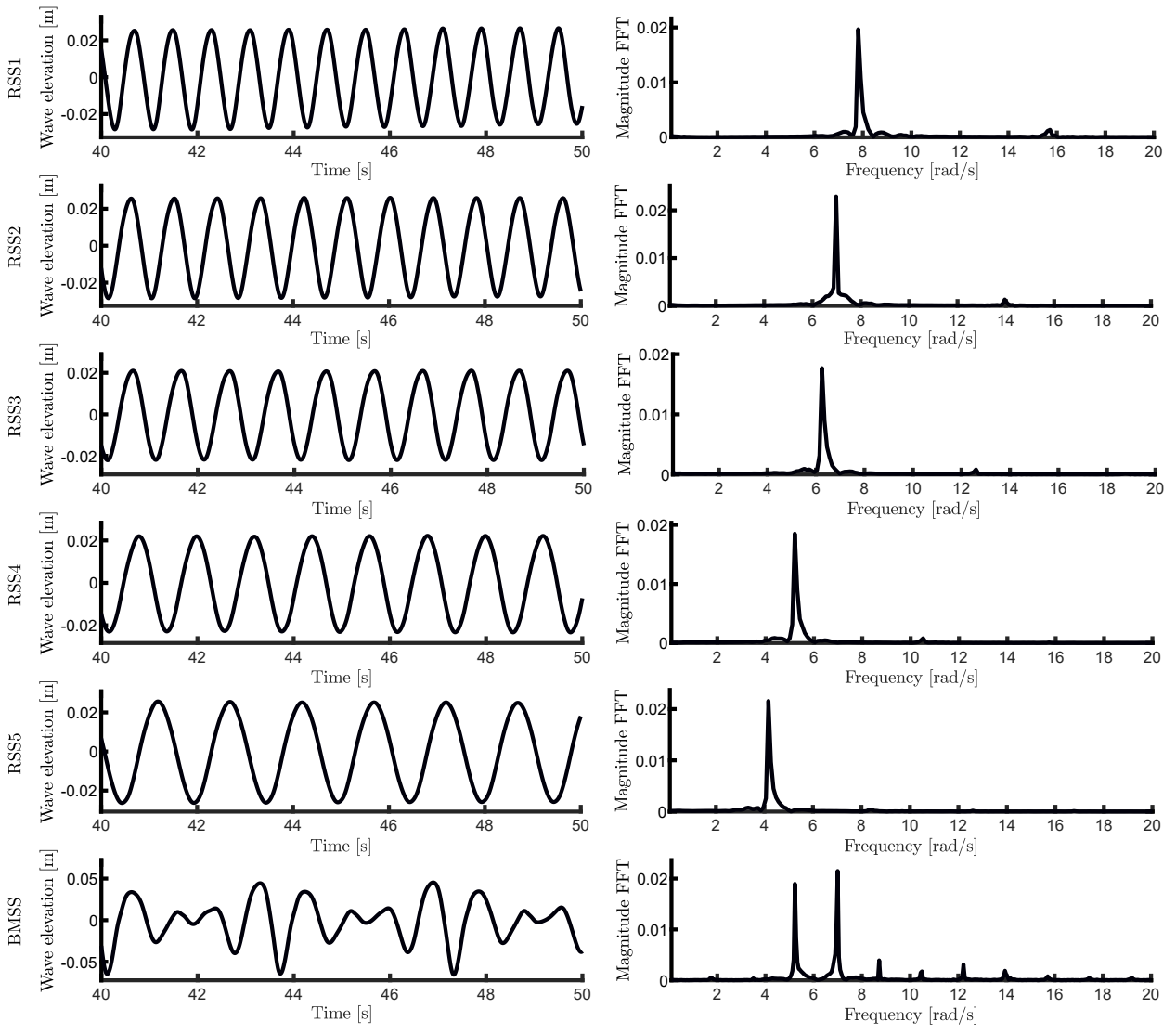

Figure 13: Test 1: Experimental free-surface elevation as measured by WP 1, both in time (left), and frequency (right), for RSS1 to RSS5 and BMSS.

happening within the wave tank which, though capable of providing a great wave absorption effort, inevitably generates small wall reflections in different directions. To illustrate this, Figure 17 presents the normalised error (NSE) w.r.t. WP 15 (consistently with the correlation in Figure 16), computed as $e_{\mathrm{WP}i} = |\eta_{\mathrm{WP}i} - \eta_{\mathrm{WP15}}| / \max|\eta_{\mathrm{WP15}}|$ for $i \in \{4, 5, 6, 7, 8, 16, 17, 18\}$ (all in row-alignment with WP 15), for the first 40 [s] of wave generation corresponding with ISS1-1. One can immediately notice that errors are always low, with maximum values (for this particular time-snippet) of approximately 5%. We further note that the choice of 'ordering' for the y-axis of Figure 17 is not arbitrary, but has a one-to-one correspondence with the wave probe placement in Figure 2. This particular ordering helps in illustrating tank reflections: While during the very first seconds all measurements are virtually identical, the error between different wave probes (w.r.t. WP 15) increases with time, and with a marked difference in space. In particular, it can be appreciated how wave reflections are coming from a specific direction in the tank for this case (ostensibly from the side corresponding with WP 8), so that the error clearly propagates in time according to the positioning of the probe (*i.e.* reflections take slightly longer to arrive to wave probes which are further away from WP 8).

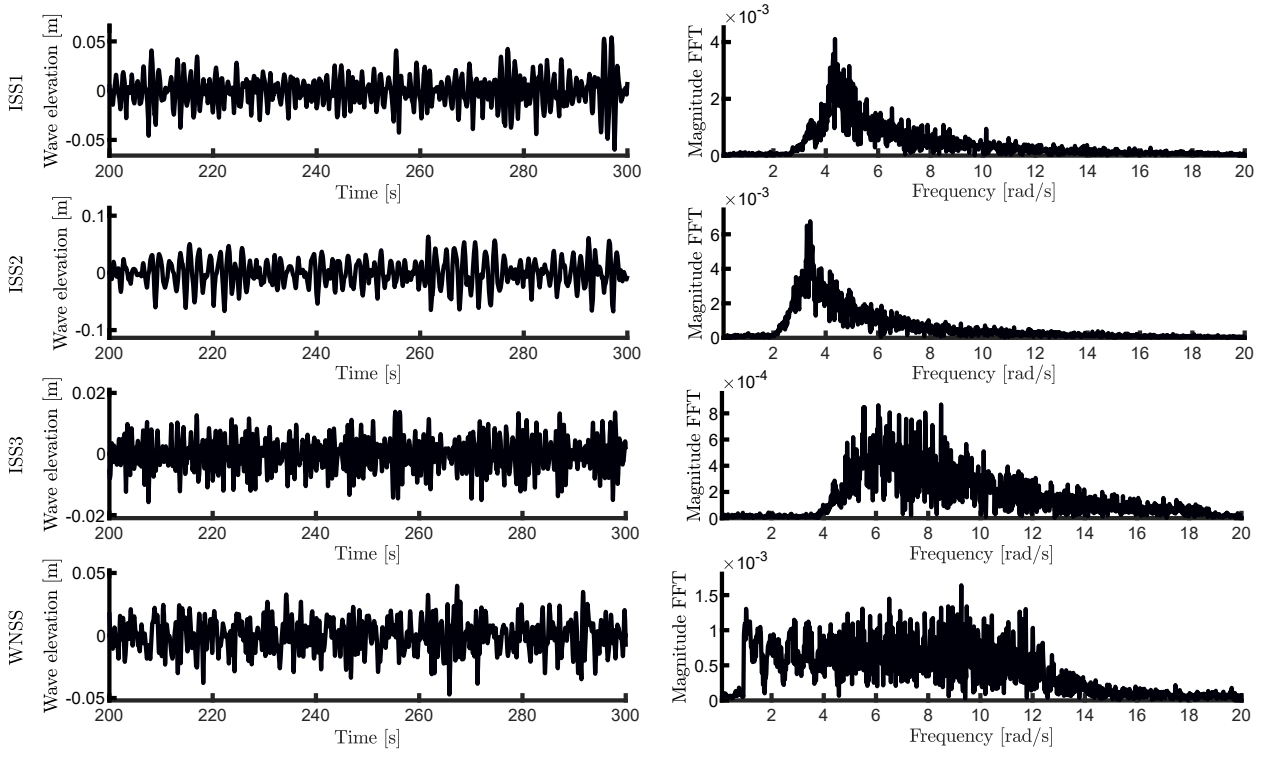

Figure 14: Test 1: Experimental free-surface elevation as measured by WP 1, both in time (left), and frequency (right), for ISS1-1 to ISS3-1 and WNSS1.

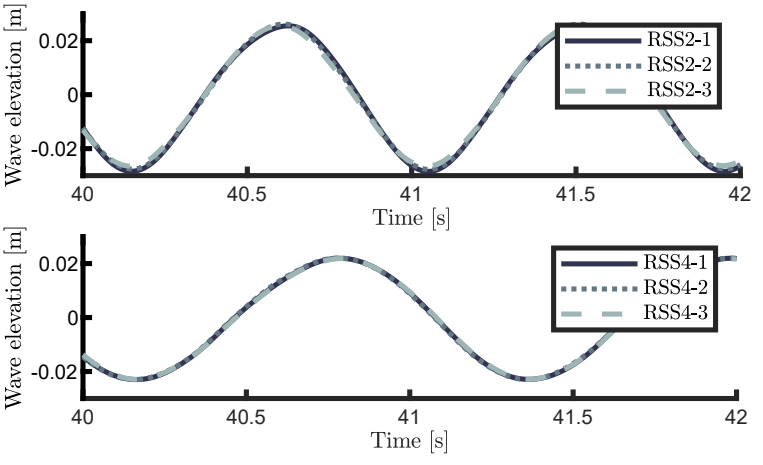

Figure 15: Realisations 1 to 3 for RSS2 (top) and RSS4 (bottom).

4.2. Test 2: Wave excitation

Following Test 1, as described in Section 4.1, we proceed to measure the so-called wave excitation force/torque acting on the different WEC array configurations, for each specific free-surface elevation generated within the wave tank, and every single layout tested. To achieve this, the devices involved in each layout are essentially blocked (each associated PTO motor shaft is locked - see *e.g.* [21]), and hence the force $f_{\mathbf{B}}$ exerted by each particular wave can be measured directly via the load cell attached to point **B** (see Section 2.2 and Figure 3), and transformed to torque w.r.t. point **A**, *i.e.* $\tau_{\mathbf{A}}$, via equation (1).

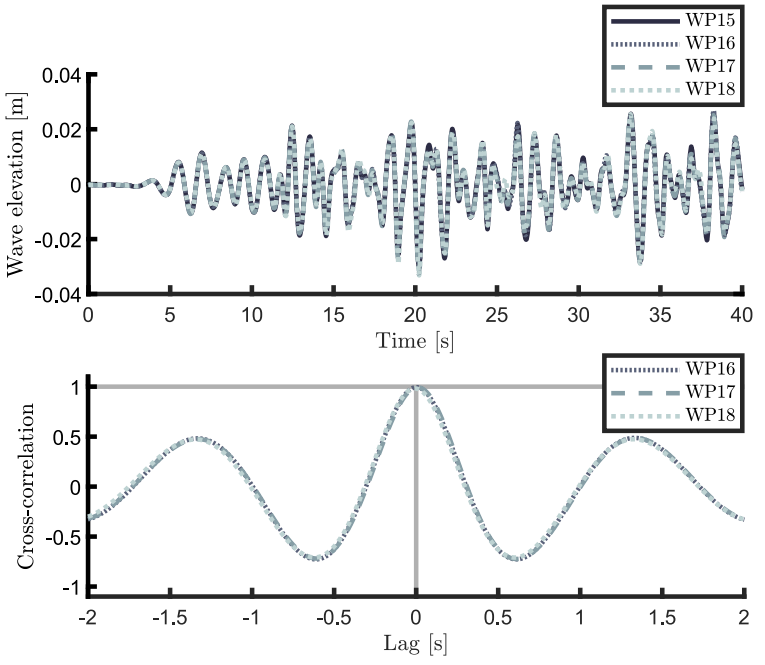

Figure 16: Free-surface elevation measurement for WP 15 to WP 18 (top), and corresponding normalised cross-correlation w.r.t. WP 15 (bottom).

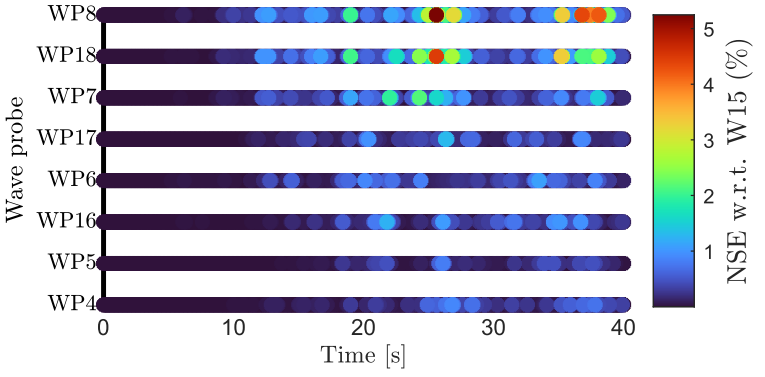

Figure 17: Set of wave probes in row-aligment, centered w.r.t. D1, D2, D3 and D4, and their corresponding normalised error against WP 15.

To briefly illustrate the nature of the measurements obtained within this test, Figure 18 shows wave excitation torque (computed about each corresponding reference point **A** in Figure 3) for L4 (layout composed of D1, D2 and D3) and L5 (layout composed of D1, D3 and D5), when the generated wave corresponds with RSS4. It can be appreciated how, while the excitation is relatively similar for all devices in L4, this changes when considering L5, given the positioning of D5 within the wave tank.

To further illustrate Test 2, Figure 19 shows wave excitation torque $\tau_{\mathbf{A}}$ for D1 in different layout configurations (L0, L1 and L4), when the generated wave within the basin corresponds to RSS4. Note that, as described in detail within Section 2.4, L0 represents the 'undisturbed' (baseline) device, *i.e.* only D1 is present in the layout configuration. L1 and L4 incorporate one (D2) and two (D2 and D3) WECs within the basin, in an adjacent configuration w.r.t. D1, hence naturally introducing interactions between devices.

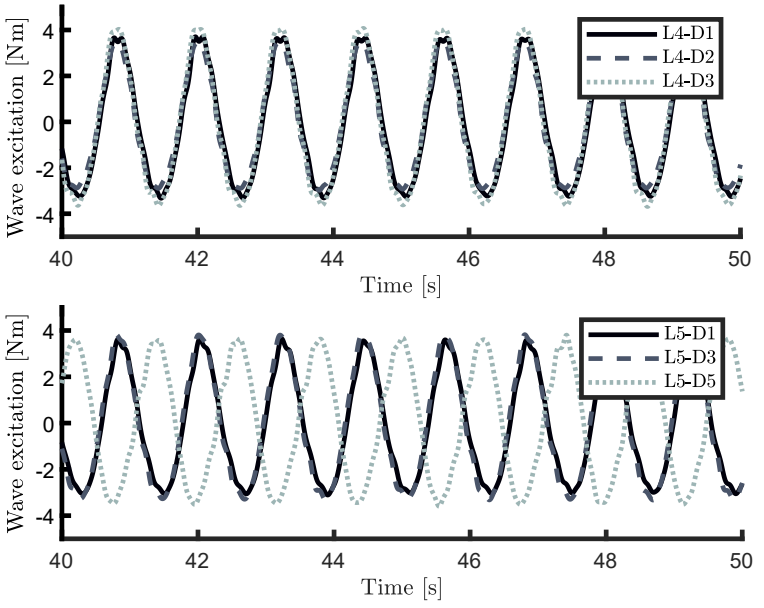

Figure 18: Wave excitation torque for L4 and L5, when RSS4 is generated within the wave basin.

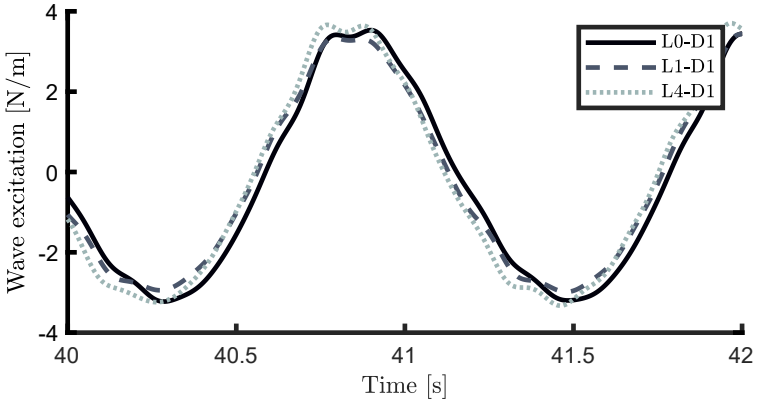

Figure 19: Wave excitation torque for D1 in different layout configurations (L0, L1 and L4), when RSS4 is generated within the wave basin.

4.3. Test 3: Uncontrolled device motion

Test 3, introduced within this section, completes the information gathered within Tests 1 and 2, by providing motion variables for each device within SWELL, in every single layout tested, and each generated wave within the basin. In particular, as described within Section 2.2, two main motion variables can be measured directly, using the instrumentation available in each device: Linear (PTO) position z_{PTO} (either via the incorporated sensor within the corresponding driver or the laser position sensor placed on top of the motor - see Section 2.2), and floater (linear) acceleration $\ddot{z}_{\mathbf{E}}$ (measured via the accelerometer placed on top of each floater). We note that, throughout the activities pertaining this particular test, the PTO reference force is set to zero, *i.e.* $u^{\text{ref}}_{\text{PTO}} = 0$ in Figure 6, effectively guaranteeing 'free' (uncontrolled) motion of the WEC system according to each generated input wave.

To have a powerful dataset, useful for a large modelling/validation activities, we aim to provide a complete description of the system motion (*i.e. displacement*, *velocity* and *acceleration*) about the reference point **A** (see Figure 3), for each layout considered. As discussed previously within Section 2.2, while $\theta_{\mathbf{A}}$ and $\ddot{\theta}_{\mathbf{A}}$ can be reconstructed straightforwardly following equation (1), $\dot{\theta}_{\mathbf{A}}$ effectively requires estimation. To do this with the available measures, we

employ standard methodologies from the field of sensor fusion, and we leverage a Kalman Filtering (KF) technique to provide estimates when needed.

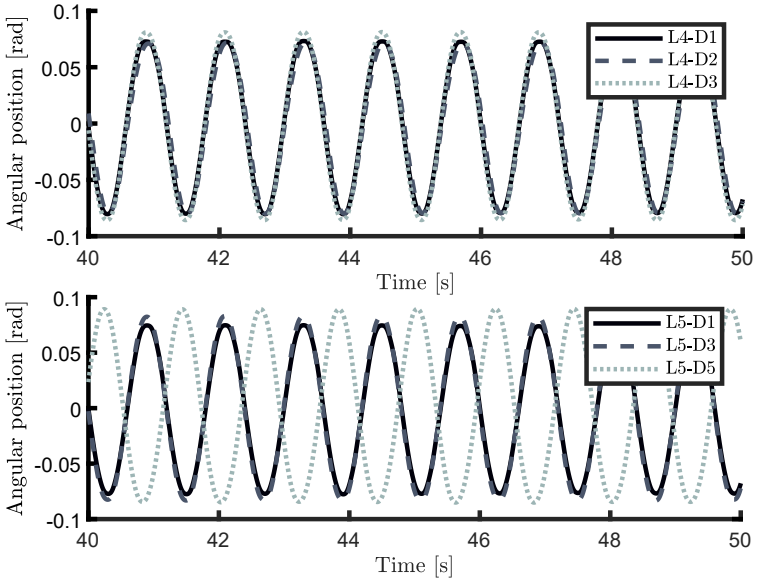

Figure 20: Motion for L4 and L5, when RSS4 is generated within the wave basin.

To illustrate the data collected via Test 3, Figure 20 shows angular positions $\theta_{\mathbf{A}}$ for every device in L4 and L5, when RSS4 is generated within the wave basin. Note that this figure is, in fact, a 'companion' of Figure 18, in the sense that the former represents the motion of the WEC prototypes when the latter (torque) is applied to each array configuration. It is interesting to see that, for this specific wave (RSS4), the devices in L4 (which are in a row-like formation) move in a synchronised fashion, *i.e.* they share virtually the same amplitude and phase in motion. This is, clearly, not necessarily the case for the remainder of the waves tested within this campaign, since the motion (and intensity of the interaction between devices in the array) intrinsically depend on the wave characteristics. For instance, Figure 21 shows $\theta_{\mathbf{A}}$ for the same configuration, *i.e.* L4, when ISS1-1 is generated within the wave tank. Note that, while D1 and D3 (which are located at the 'end-points' of the layout) behave almost identically, D2 (sitting in between D1 and D3) presents a very different motion, due to the effect of the interaction between devices. Finally, to further complete the results illustrated within this section, Figure 22 presents $\theta_{\mathbf{A}}$ for D1 in different layout configurations (L0, L1 and L4), when the generated wave within the basin corresponds to RSS4. Note that, as in the case of Figures 20 and 18, Figure 22 represents the 'companion' of Figure 19, being wave excitation torque/device motion pairs.

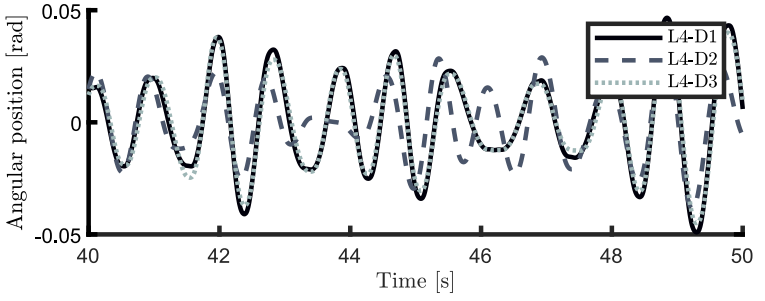

Figure 21: Motion for L4, when ISS1-1 is generated within the wave basin.

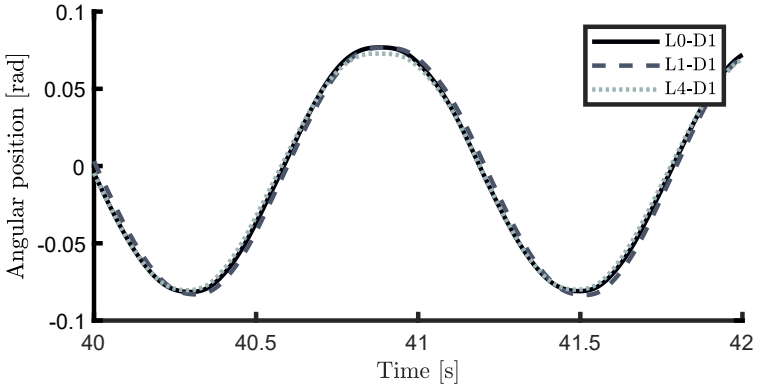

Figure 22: Motion for D1 in different layouts (L0, L1 and L4), when RSS4 is generated within the wave basin.

Table 5
Passive and reactive control parameters for each sea state considered within Test 4.

SS	**Passive** (P)	**Reactive** (PI)	
	ϕ^{P} [Nms/rad]	ϕ^{PI} [Nms/rad]	ψ^{PI} [Nm/rad]
ISS1	9.57	2.74	-32.31
ISS2	16.74	4.14	-24.73
ISS3	2.81	2.79	-2.59

4.4. Test 4: Controlled device motion

While Test 3, as described in Section 4.3, provides information on the motion associated with each WEC layout, the test is performed without the presence of an energy-maximising PTO control force/torque in the system, *i.e.* with $u^{\mathrm{ref}}_{\mathrm{PTO}} = 0$ in Figure 6. As it is well-established within the literature, and discussed within Section 1, WEC systems require tailored control technology to enhance energy extraction in operating conditions, so as to minimise the associated LCoE. When optimally designed, these control systems tend to exaggerate device motion (see [50]), potentially triggering nonlinear effects which are not present/dominant when in uncontrolled conditions.

As such, validated models, capable of representing WEC systems under the action of energy-maximising control (see the lower block in Figure 6), are effectively fundamental for accurate and reliable performance assessment of both single and array configurations. With this in mind, Test 4 incorporates in SWELL information of a subset of the WEC layouts and sea states considered within this campaign (see Table 4), under diverse control conditions. In particular, two well-known and widely-adopted control architectures are considered, often referred to, in the literature, as *passive* (proportional - P), and *reactive* (proportional-integral - PI) controllers, *i.e.*

$$\begin{aligned} &(\mathrm{P}): \quad \tau^{\mathrm{ref}}_{\mathrm{PTO}} = \phi^{\mathrm{P}}\dot{\theta}_{\mathbf{A}}, \\ &(\mathrm{PI}): \quad \tau^{\mathrm{ref}}_{\mathrm{PTO}} = \phi^{\mathrm{PI}}\dot{\theta}_{\mathbf{A}} + \psi^{\mathrm{PI}}\theta_{\mathbf{A}}, \end{aligned} \tag{2}$$

where the set of parameters $\Phi = \{\phi^{\mathrm{P}}, \phi^{\mathrm{PI}}, \psi^{\mathrm{PI}}\} \subset \mathbb{R}$ is computed in terms of the so-called impedance-matching (also referred to complex-conjugate - see *e.g.* [17, 72]) condition for WEC systems, using the frequency-response map of L0 (*i.e.* a single device - D1) as benchmark. The specific values for the set of parameters Φ, which are given explicitly for completeness within Table 5, naturally depend on the generated wave condition (see the discussion provided in *e.g.* [72]), and are equally considered for all the devices and layouts tested, for consistency of the dataset, hence allowing a direct comparison between different array configurations. Note that $\tau^{\mathrm{ref}}_{\mathrm{PTO}}$ can be mapped to a corresponding force $u^{\mathrm{ref}}_{\mathrm{PTO}}$ by simply employing the relations presented in equation (1).

To illustrate the results obtained within this test, Figure 23 presents motion $\theta_{\mathbf{A}}$ for L0, in uncontrolled (solid), passively- (dashed), and reactively-controlled (dotted) conditions, for ISS1-1. As it can be appreciated, both passive and reactive cases clearly present different closed-loop dynamics, with the latter generating both larger control torque requirements, and effective device motion, in line with the discussion provided within the first paragraph of this section

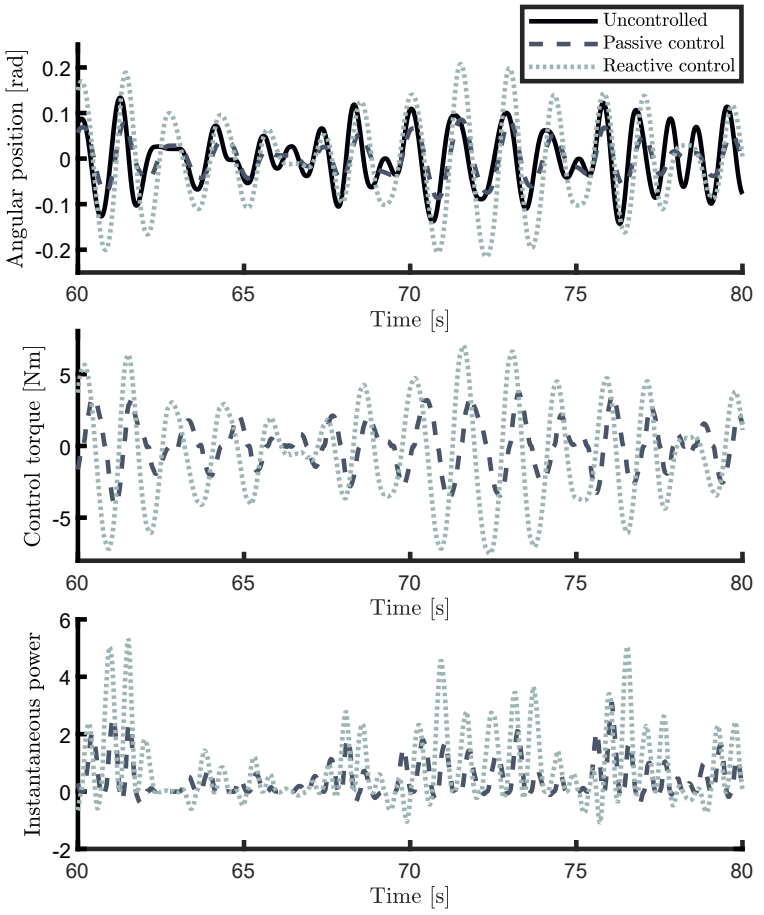

Figure 23: Controlled behaviour for L0 when ISS1-1 is generated within the basin.

(see also Section 1). Note that, clearly, the reactive controller requires negative instantaneous power flow, injecting energy into the WEC system at specific time instants to maximise the total absorbed power [17]. To further emphasise the fact that devices under controlled conditions can present larger motions than those in uncontrolled scenarios, Figure 24 illustrates a time-snippet of uncontrolled and reactively-controlled angular displacement $\theta_{\mathbf{A}}$ for L4, when ISS1-1 is generated within the wave basin. Notice that all three devices involved (D1, D2 and D3) present larger displacement values in the reactive control case, consistent with the presented discussion.

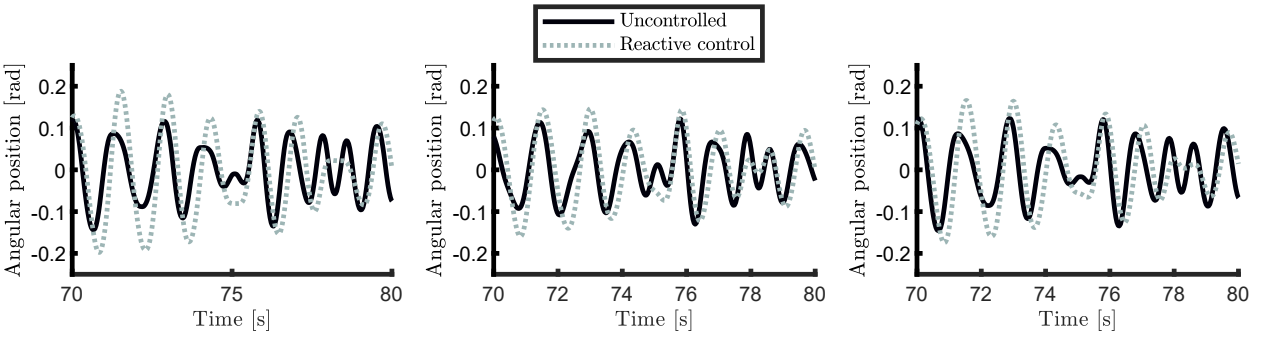

Figure 24: Controlled behaviour for L4 when ISS1-1 is generated within the basin.

4.5. Synergy between tests

Tests 1 to 4 have been all designed with a pre-defined synergy, so as to facilitate a dataset to the WEC community able to provide enough information to perform a large number of data-based modelling/validation tasks for array configurations. The main synergies between these tests can be appreciated in the schematic presented within Figure 25, and are detailed in the paragraphs below.

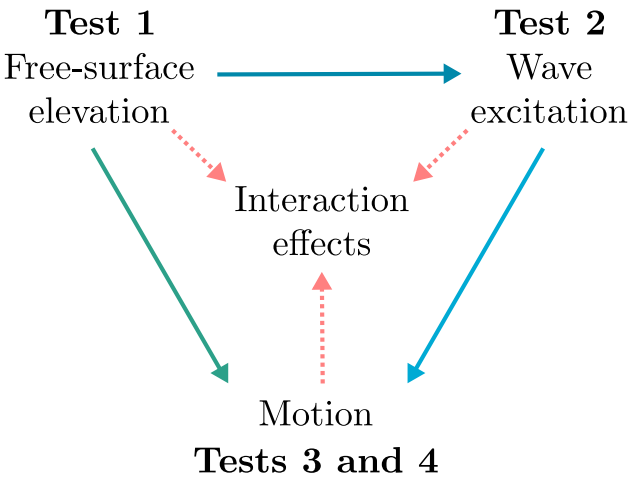

Figure 25: Schematic diagram indicating synergy between different tests.

Tests 1 and 2 provide information for data-based modelling/validation of free-surface-elevation-to-wave-excitation dynamics (path indicated with dark-blue in Figure 25). For instance, exploiting the data provided by the wave probes placed in the central position of each device (as collected in Test 1), and the corresponding wave excitation force/torque (recovered from Test 2), one can directly characterise/validate the free-surface-to-excitation dynamics of each device and layout considered. In particular, the set of white noise sea states (WNSS1, WNSS2 and WNSS3) is particularly useful for this task, being able to provide information for such a mapping in a large operational bandwidth. By way of example, Figure 26 presents an empirical frequency-domain characterisation of the free-surface-elevation-to-wave-excitation-torque dynamics associated with L0 (*i.e.* D1), in terms of the so-called empirical transfer function estimate (ETFE - see *e.g.* [21, 68]). This map has been computed using the free-surface elevation measured at the central position of D1 as input set, for all three white noise sea states (as in Test 1), and their associated measured wave excitation torque (as in Test 2).

Following an analogous procedure, Tests 2 and 3 can be used to characterise/validate the excitation-to-motion dynamics (path indicated with light-blue in Figure 25). This is illustrated in Figure 27, which presents the corresponding ETFE for L0, computed using the set of excitation torques for WNSS1 to WNSS3 (as measured in Test 2), and their corresponding uncontrolled motion (as per Test 3). Finally, note that, using Tests 1 and 3, one can also characterise/validate the behaviour of the tested WEC array layouts from the free-surface elevation to the corresponding device motion (path indicated with green in Figure 25).

The methodology discussed in the paragraphs immediately above can be also performed in energy-maximising control conditions, by exploiting the information provided within Test 4. In particular, combining Tests 1 and 2, with the outputs generated in Test 4, the dataset contains information to model/validate the dynamics of WEC array numerical models in controlled conditions, for different layout configurations, being this fundamental for reliable performance assessment of WEC farm technology. Finally, with suitable combinations of the information gathered in Tests 1, 2, 3 and 4 (as schematically indicated within Figure 25), one can also validate models for device interaction, and proximal and distal wave fields. In particular, the large number of wave probes available throughout the experiments (see Figure 2) allows for a detailed numerical description of the interaction between devices and resulting wave field, for all the layout configurations tested within this campaign.

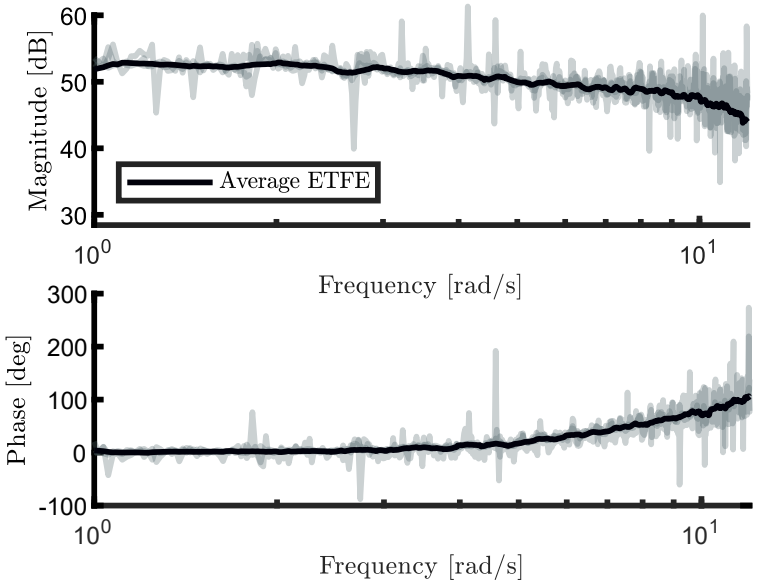

Figure 26: Free-surface-elevation-to-wave-excitation-torque ETFE for L0, computed using WNSS1, WNSS2 and WNSS3. The black line indicates the average over the three I/O experiments.

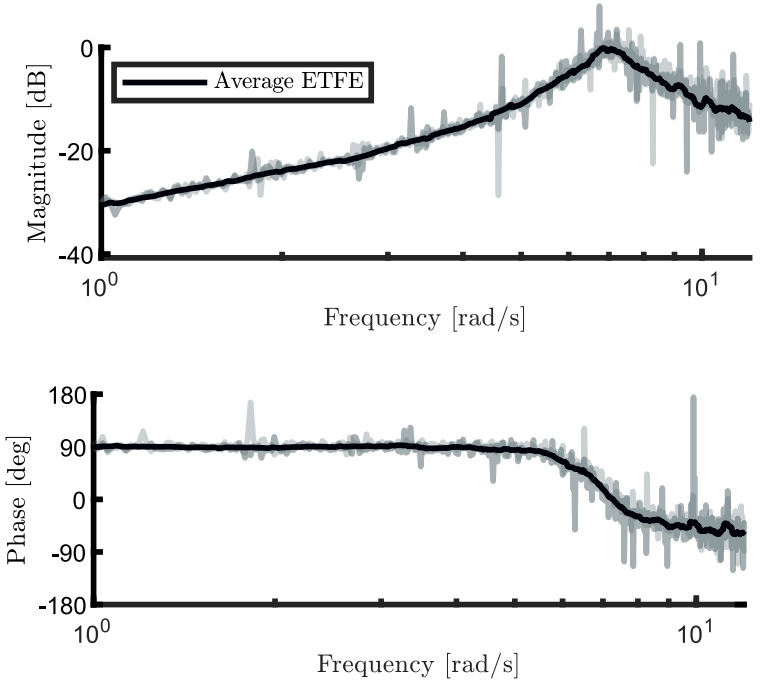

Figure 27: Wave-excitation-to-angular-velocity ETFE for L0, computed using WNSS1, WNSS2 and WNSS3. The black line indicates the average over the three I/O experiments.

5. Dataset specification

This section is devoted to provide a description of the dataset included within this paper, *i.e.* SWELL, composed of the data collected in the tests described in Section 4. The directory structure, associated with SWELL, can be appreciated in Figure 28. In particular, two main folders can be found within the structure, namely `Tests` and `Linear motors`. The former contains the core of the dataset, including data from Tests 1 to 4 (as described in

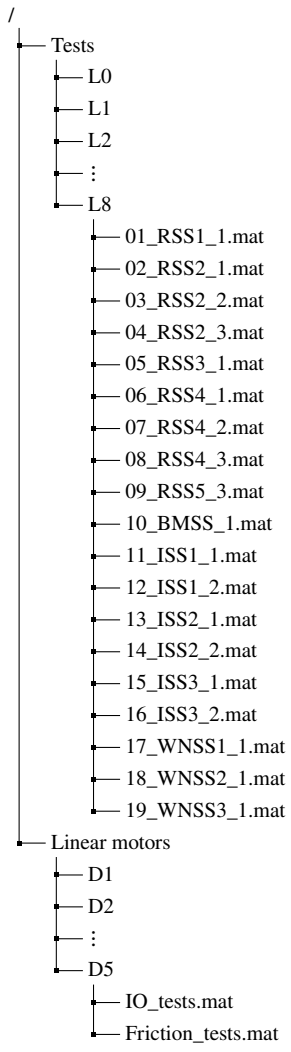

Figure 28: Directory structure for SWELL.

Section 4), for every WEC array layout involved. The latter, instead, is composed of the data characterising each PTO linear motor, in line with the discussion provided in Section 2.5.

SWELL is fully composed of MATLAB-compatible files, in the native format '`.mat`'. This is done with the aim of maximising the impact of the dataset, providing files ready to be processed and analysed promptly. The totality of the data is stored in a standard matrix format (with dimensions as clarified in the following paragraphs), hence avoiding any potential compatibility issues between diverse MATLAB software versions/releases. We further note that '`.mat`' files can be opened straightforwardly using *e.g.* PYTHON or OCTAVE, being hence also compatible with a wide set of analysis tools outside MATLAB.

We begin with a description of the main part of the directory, *i.e.* `Tests`, which contains 9 folders, each corresponding with one of the 9 layouts tested (*i.e.* from L0 to L8). Inside each of these folders, 19 files with extension '`.mat`' can be found, each linked with a single operating condition, *i.e.* sea state and realisation (if applicable). For instance, '`01_RSS1_1.mat`' refers to results for RSS1 realisation 1 (note that a single realisation of RSS1 is effectively considered within the campaign - see Table 3), while *e.g.* '`16_ISS3_2.mat`' refers to ISS3, realisation 2.

Referring to the content related to these latter 9 folders, within each of these '`.mat`' files, as listed in Figure 28, a number of variables can be found, associated with the results obtained from Tests 1 to 4, for each layout considered. The complete set of variables can be appreciated in Table 6, including associated test, name in file, description, units,

and effective variable dimensions, where $\{N_t, N_d\} \subset \mathbb{N}$ refer to the length of the time vector and number of devices present in the layout, respectively. Note that, the variables related to Tests 1 to 3 are effectively present in the totality of the '`.mat`' files included within the dataset, while those related to Tests 4 and 5 are exclusive to layouts L0 to L5 (see also Table 4).

The time vector, as specified within Table 6, is common to all tests and variables, *i.e.* all variables have been synchronised and interpolated w.r.t. a single reference time vector, for each '`.mat`' file within the main folder `Tests`. This has been possible by exploiting a trigger output signal available within the wavemaker system of Aalborg University, which provides a digital flag at the precise moment wave generation starts/ends. Apart from synchronisation, we have filtered the signals accordingly, to avoid noise pollution within the dataset. In particular, to achieve such an objective, a zero-phase (forward-backward) Chebyshev filter (see *e.g.* [66]) has been applied to all variables involved in Table 6, with a filter order 4 and a (sufficiently large) cut-off frequency of 50 [rad/s].

Finally, and related to the PTO characterisation discussed within Section 2.5, the folder `Linear motors` contains information regarding each linear (PTO) motor, for D1 to D5. In particular, two '`.mat`' files can be found within each device folder, namely `IO_tests.mat` and `Friction_tests.mat`. As detailed within Table 7, the former file contains I/O information for each single motor, where the reference force (input) is a chirp signal with different amplitudes (see Figure 7). In contrast, the latter features the friction tests described in Section 2.5 (and illustrated in Figure 8), including all motion variables required to characterise these effects numerically (see Table 8).

6. Conclusions

We provide, in this paper, a detailed account of an experimental campaign designed with the sole objective of providing an open-access dataset for arrays of wave energy conversion systems, termed SWELL, hence facilitating a crucial resource for model validation and data-based modelling. The campaign, executed within the wave basin facilities available at Aalborg University, is composed of 4 essential tests with a pre-designed synergy, aimed at maximising the value of the information available within SWELL for the WEC development community. In particular, key variables, such as free-surface elevation at different points within the basin (Test 1), wave excitation force (Test 2), uncontrolled motion (Test 3), and behaviour under energy-maximising (passive and reactive) control conditions (Test 4), are effectively included as part of the dataset, for each of the sea states, devices, and layouts considered. Furthermore, a characterisation of each PTO system is also presented, by means of I/O and friction tests. This is, to the best of our knowledge, the largest open-access dataset characterising arrays of WEC systems available in the literature, including a wide variety of WEC layouts, realistic PTO effects (including energy-maximising control), tested in different scenarios following a consistent protocol, designed to suit the needs associated with a vast number of modelling tasks. SWELL provides, hence, an essential resource for reliability assessment of diverse numerical modelling approaches, supporting efficient decision making, and contributing to the pathway towards effective commercialisation of ocean wave energy.

ACKNOWLEDGMENT

The authors are grateful with Dr. M. Folley, from Queen's University Belfast, for his valuable input during the execution of the experimental campaign. The support of Dr. S. Wood, which has been fundamental for setup of the data acquisition system, is also appreciated by the authors. This project has received funding from the European Union's Horizon 2020 research and innovation programme under the Marie Sklodowska-Curie grant agreements No 101024372 and 101034297, and support from the framework COST Action 17105 - WECANet. The support of the Facultad de Ingeniería, Universidad Nacional de La Plata (UNLP), CONICET, and Agencia I+D+i from Argentina, is also acknowledged.

References

[1] Energy Information Administration (EIA). International energy outlook. Technical report, EIA, Washington, United States, 2019.
[2] European Commission. Energy roadmap 2050: Impact assessment and scenario analysis. Technical report, European Commission, Brussels, Belgium, 2011.
[3] European Commission. A policy framework for climate and energy in the period 2020 to 2030. Technical report, European Commission, Brussels, Belgium, 2014.
[4] European Commission. The european green deal. Technical report, European Commission, Brussels, Belgium, 2019.
[5] European Commission. Repowereu. Technical report, European Commission, Brussels, Belgium, 2022.

Table 6
Variables for Tests 1 to 4, contained within the dataset.

	Name	Description	Units	Dim.
All tests	*time*	Time vector (common to all variables)	s	$1 \times N_t$
Test 1	*waveElevation_UD*	Wave elevation in all probe locations (1 to 19)	m	$19 \times N_t$
Test 2	*waveElevation_WE*	Wave elevation in probes 1 to 14	m	$14 \times N_t$
	excitationForce_WE	Wave excitation force (w.r.t. point **B**)	N	$N_d \times N_t$
	excitationTorque_WE	Wave excitation torque (w.r.t. point **A**)	Nm	$N_d \times N_t$
Test 3	*waveElevation_UM*	Wave elevation in probes 1 to 14	m	$14 \times N_t$
	motorPos_UM	Position of linear motor (as measured by motor driver)	m	$N_d \times N_t$
	laserPos_UM	Position of linear motor (as measured by laser sensor)	m	$N_d \times N_t$
	motorVel_UM	Velocity of linear motor (as estimated by motor driver)	m/s	$N_d \times N_t$
	accelerometerAcc_UM	Acceleration w.r.t. point **E** (as measured by accelerometer)	m/s^2	$N_d \times N_t$
	angularPos_UM	Angular position w.r.t. point **A**	rad	$N_d \times N_t$
	angularVel_UM	Angular velocity w.r.t. point **A** (output of KF)	rad/s	$N_d \times N_t$
	angularAcc_UM	Angular acceleration w.r.t. point **A**	rad/s^2	$N_d \times N_t$
Test 4	*waveElevation_CM_P*	Wave elevation in probes 1 to 14 under P control	m	$14 \times N_t$
	motorPos_UM_P	Position of linear motor (as measured by motor driver) under P control	m	$N_d \times N_t$
	laserPos_UM_P	Position of linear motor (as measured by laser sensor) under P control	m	$N_d \times N_t$
	motorVel_UM_P	Velocity of linear motor (as estimated by motor driver) under P control	m/s	$N_d \times N_t$
	accelerometerAcc_UM_P	Acceleration w.r.t. point **E** (as measured by accelerometer) under P control	m/s^2	$N_d \times N_t$
	angularPos_UM_P	Angular position w.r.t. point **A** under P control	rad	$N_d \times N_t$
	angularVel_UM_P	Angular velocity w.r.t. point **A** (output of KF) under P control	rad/s	$N_d \times N_t$
	angularAcc_UM_P	Angular acceleration w.r.t. point **A** under P control	rad/s^2	$N_d \times N_t$
	controlForce_UM_P	Requested control force (reference to motor driver) w.r.t. point **B** under P control	N	$N_d \times N_t$
	controlTorque_UM_P	Requested control torque (reference to motor driver) w.r.t. point **A** under P control	Nm	$N_d \times N_t$
	waveElevation_CM_PI	Wave elevation in probes 1 to 14 under PI control	m	$14 \times N_t$
	motorPos_UM_PI	Position of linear motor (as measured by motor driver) under PI control	m	$N_d \times N_t$
	laserPos_UM_PI	Position of linear motor (as measured by laser sensor) under PI control	m	$N_d \times N_t$
	motorVel_UM_PI	Velocity of linear motor (as estimated by motor driver) under PI control	m/s	$N_d \times N_t$
	accelerometerAcc_UM_PI	Acceleration w.r.t. point **E** (as measured by accelerometer) under PI control	m/s^2	$N_d \times N_t$
	angularPos_UM_PI	Angular position w.r.t. point **A** under PI control	rad	$N_d \times N_t$
	angularVel_UM_PI	Angular velocity w.r.t. point **A** (output of KF) under PI control	rad/s	$N_d \times N_t$
	angularAcc_UM_PI	Angular acceleration w.r.t. point **A** under PI control	rad/s^2	$N_d \times N_t$
	controlForce_UM_PI	Requested control force (reference to motor driver) w.r.t. point **B** under PI control	N	$N_d \times N_t$
	controlTorque_UM_PI	Requested control torque (reference to motor driver) w.r.t. point **A** under PI control	Nm	$N_d \times N_t$

Table 7
Variables for PTO I/O tests, contained within the dataset.

Name	Description	Units	Dim.
time	Time vector (common to all variables)	s	$1 \times N_t$
referenceForce_chirp_1	Requested chirp test force (1) (reference to motor driver) w.r.t. point **B** (amplitude 15 [N])	N	$1 \times N_t$
measuredForce_chirp_1	Force w.r.t. point **B** (as measured by load cell) for chirp test force (1)	N	$1 \times N_t$
referenceForce_chirp_2	Requested chirp test force (2) (reference to motor driver) w.r.t. point **B** (amplitude 17.5 [N])	N	$1 \times N_t$
measuredForce_chirp_2	Force w.r.t. point **B** (as measured by load cell) for chirp test force (2)	N	$1 \times N_t$

Table 8
Variables for PTO friction tests, contained within the dataset.

Name	Description	Units	Dim.
time	Time vector (common to all variables)	s	$1 \times N_t$
motorPos	Position of linear motor (as measured by motor driver)	m	$1 \times N_t$
motorVel	Velocity of linear motor (as estimated by motor driver)	m/s	$1 \times N_t$
accelerometerAcc	Acceleration w.r.t. point **E** (as measured by accelerometer)	m/s^2	$1 \times N_t$
loadcellForce	Force w.r.t. point **B** (as measured by load cell)	N	$1 \times N_t$

[6] Gunnar Mork, Stephen Barstow, Alina Kabuth, and M Teresa Pontes. Assessing the global wave energy potential. In *International Conference on Offshore Mechanics and Arctic Engineering*, volume 49118, pages 447–454, 2010.

[7] Kester Gunn and Clym Stock-Williams. Quantifying the global wave power resource. *Renewable Energy*, 44:296–304, 2012.

[8] BG Reguero, IJ Losada, and FJ Méndez. A global wave power resource and its seasonal, interannual and long-term variability. *Applied Energy*, 148:366–380, 2015.

[9] Michael E McCormick. *Ocean wave energy conversion*. Courier Corporation, 2013.

[10] Iraide López, Jon Andreu, Salvador Ceballos, Iñigo Martínez De Alegría, and Iñigo Kortabarria. Review of wave energy technologies and the necessary power-equipment. *Renewable and sustainable energy reviews*, 27:413–434, 2013.

[11] Wataru Sasaki. Predictability of global offshore wind and wave power. *International Journal of Marine Energy*, 17:98–109, 2017.

[12] Olivia Langhamer, Kalle Haikonen, and Jan Sundberg. Wave power—sustainable energy or environmentally costly? a review with special emphasis on linear wave energy converters. *Renewable and Sustainable Energy Reviews*, 14(4):1329–1335, 2010.

[13] Andrea E Copping, Lenaïg G Hemery, Dorian M Overhus, Lysel Garavelli, Mikaela C Freeman, Jonathan M Whiting, Alicia M Gorton, Hayley K Farr, Deborah J Rose, and Levy G Tugade. Potential environmental effects of marine renewable energy development—the state of the science. *Journal of Marine Science and Engineering*, 8(11):879, 2020.

[14] David Ross. *Power from the Waves*. Oxford University Press, USA, 1995.

[15] Bingyong Guo and John V Ringwood. A review of wave energy technology from a research and commercial perspective. *IET Renewable Power Generation*, 15(14):3065–3090, 2021.

[16] Ali Trueworthy and Bryony DuPont. The wave energy converter design process: Methods applied in industry and shortcomings of current practices. *Journal of Marine Science and Engineering*, 8(11):932, 2020.

[17] John V Ringwood, Giorgio Bacelli, and Francesco Fusco. Energy-maximizing control of wave-energy converters: The development of control system technology to optimize their operation. *IEEE control systems magazine*, 34(5):30–55, 2014.

[18] Nicolás Faedo, Sébastien Olaya, and John V Ringwood. Optimal control, mpc and mpc-like algorithms for wave energy systems: An overview. *IFAC Journal of Systems and Control*, 1:37–56, 2017.

[19] Aurélien Babarit and Alain H Clément. Optimal latching control of a wave energy device in regular and irregular waves. *Applied Ocean Research*, 28(2):77–91, 2006.

[20] Nicolás Faedo, Demián García-Violini, Yerai Peña-Sanchez, and John V Ringwood. Optimisation-vs. non-optimisation-based energy-maximising control for wave energy converters: A case study. In *2020 European Control Conference (ECC)*, pages 843–848. IEEE, 2020.

[21] Nicolás Faedo, Yerai Peña-Sanchez, Demián García-Violini, Francesco Ferri, Giuliana Mattiazzo, and John V Ringwood. Experimental assessment and validation of energy-maximising moment-based optimal control for a prototype wave energy converter. *Control Engineering Practice*, 133:105454, 2023.

[22] John V Ringwood. Wave energy control: status and perspectives 2020. *IFAC-PapersOnLine*, 53(2):12271–12282, 2020.

[23] Malin Göteman, Marianna Giassi, Jens Engström, and Jan Isberg. Advances and challenges in wave energy park optimization—a review. *Frontiers in Energy Research*, 8:26, 2020.

[24] Bryson Robertson, Clayton Hiles, Ewelina Luczko, and Bradley Buckham. Quantifying wave power and wave energy converter array production potential. *International Journal of Marine Energy*, 14:143–160, 2016.

[25] Kelley Ruehl and Diana Bull. Wave energy development roadmap: Design to commercialization. In *2012 Oceans*, pages 1–10, 2012.

[26] J Hodges, J Henderson, L Ruedy, M Soede, J Weber, P Ruiz-Minguela, H Jeffrey, E Bannon, M Holland, R Maciver, et al. An international evaluation and guidance framework for ocean energy technology. Technical report, International Energy Agency - Ocean Energy Systems (IEA-OES), Lisbon, Portugal, 2021.

[27] Aurélien Babarit. On the park effect in arrays of oscillating wave energy converters. *Renewable Energy*, 58:68–78, 2013.

[28] Mathew BR Topper, Vincenzo Nava, Adam J Collin, David Bould, Francesco Ferri, Sterling S Olson, Ann R Dallman, Jesse D Roberts, Pablo Ruiz-Minguela, and Henry F Jeffrey. Reducing variability in the cost of energy of ocean energy arrays. *Renewable and Sustainable Energy Reviews*, 112:263–279, 2019.

[29] Matt Folley, Aurélien Babarit, Ben Child, David Forehand, Louise O'Boyle, Katie Silverthorne, Johannes Spinneken, Vasiliki Stratigaki, and Peter Troch. A review of numerical modelling of wave energy converter arrays. In *International Conference on Offshore Mechanics and Arctic Engineering*, volume 44946, pages 535–545. American Society of Mechanical Engineers, 2012.

[30] Reduan Atan, William Finnegan, Stephen Nash, and Jamie Goggins. The effect of arrays of wave energy converters on the nearshore wave climate. *Ocean Engineering*, 172:373–384, 2019.

[31] Jochem Weber. Wec technology readiness and performance matrix–finding the best research technology development trajectory. In *Proceedings of the 4th International Conference on Ocean Energy, Dublin, Ireland*, volume 17, 2012.

[32] Matt Folley. *Numerical modelling of wave energy converters: state-of-the-art techniques for single devices and arrays*. Academic Press, 2016.

[33] Josh Davidson and Ronan Costello. Efficient nonlinear hydrodynamic models for wave energy converter design—a scoping study. *Journal of Marine Science and Engineering*, 8(1):35, 2020.

[34] Johannes Falnes. *Ocean Waves and Oscillating Systems: Linear Interactions Including Wave-Energy Extraction*. Cambridge University Press, 2002.

[35] Meng Han, Feifei Cao, Hongda Shi, Hailei Kou, Haoxiang Gong, and Cui Wang. Parametrical study on an array of point absorber wave energy converters. *Ocean Engineering*, 272:113857, 2023.

[36] Malin Göteman, Jens Engström, Mikael Eriksson, and Jan Isberg. Fast modeling of large wave energy farms using interaction distance cut-off. *Energies*, 8(12):13741–13757, 2015.

[37] Nicolás Faedo, Giordano Scarciotti, Alessandro Astolfi, and John V Ringwood. Energy-maximising moment-based constrained optimal control of ocean wave energy farms. *IET Renewable Power Generation*, 15(14):3395–3408, 2021.

[38] Gael Verao Fernandez, Philip Balitsky, Vasiliki Stratigaki, and Peter Troch. Coupling methodology for studying the far field effects of wave energy converter arrays over a varying bathymetry. *Energies*, 11(11):2899, 2018.

[39] Guanghua He, Zhengxiao Luan, Ruijia Jin, Wei Zhang, Wei Wang, Zhigang Zhang, Penglin Jing, and Pengfei Liu. Numerical and experimental study on absorber-type wave energy converters concentrically arranged on an octagonal platform. *Renewable Energy*, 188:504–523, 2022.

[40] Brecht Devolder, Pieter Rauwoens, and Peter Troch. Numerical simulation of an array of heaving floating point absorber wave energy converters using openfoam. In *7th International Conference on Computational Methods in Marine Engineering (MARINE)*, pages 777–788, 2017.

[41] Brecht Devolder, Vasiliki Stratigaki, Peter Troch, and Pieter Rauwoens. Cfd simulations of floating point absorber wave energy converter arrays subjected to regular waves. *Energies*, 11(3):641, 2018.

[42] DTOcean+: Advanced Design Tools for Ocean Energy Systems Innovation, Development and Deployment. https://www.dtoceanplus.eu/. Accessed: 2023-05-03.

[43] Josh Davidson, Simone Giorgi, and John V Ringwood. Linear parametric hydrodynamic models for ocean wave energy converters identified from numerical wave tank experiments. *Ocean Engineering*, 103:31–39, 2015.

[44] Timothy Vervaet, Vasiliki Stratigaki, Francesco Ferri, Louis De Beule, Hendrik Claerbout, Bono De Witte, Marc Vantorre, and Peter Troch. Experimental modelling of an isolated wecfarm real-time controllable heaving point absorber wave energy converter. *Journal of Marine Science and Engineering*, 10(10):1480, 2022.

[45] Fabian Wendt, Kim Nielsen, Yi-Hsiang Yu, Harry Bingham, Claes Eskilsson, Morten Kramer, Aurélien Babarit, Tim Bunnik, Ronan Costello, Sarah Crowley, et al. Ocean energy systems wave energy modelling task: Modelling, verification and validation of wave energy converters. *Journal of Marine Science and Engineering*, 7(11):379, 2019.

[46] Morten Bech Kramer, Jacob Andersen, Sarah Thomas, Flemming Buus Bendixen, Harry Bingham, Robert Read, Nikolaj Holk, Edward Ransley, Scott Brown, Yi-Hsiang Yu, et al. Highly accurate experimental heave decay tests with a floating sphere: A public benchmark dataset for model validation of fluid–structure interaction. *Energies*, 14(2):269, 2021.

[47] OPERA: Open Sea Operating Experience to Reduce Wave Energy Cost. http://opera-h2020.eu/. Accessed: 2023-05-03.

[48] Vasiliki Stratigaki, Peter Troch, Tim Stallard, David Forehand, Jens Peter Kofoed, Matt Folley, Michel Benoit, Aurélien Babarit, and Jens Kirkegaard. Wave basin experiments with large wave energy converter arrays to study interactions between the converters and effects on other users in the sea and the coastal area. *Energies*, 7(2):701–734, 2014.

[49] WECwakes Project. https://www.wecanet.eu/databases. Accessed: 2023-02-14.

[50] Christian Windt, Nicolás Faedo, Markel Penalba, Frederic Dias, and John V Ringwood. Reactive control of wave energy devices–the modelling paradox. *Applied Ocean Research*, 109:102574, 2021.

[51] Rico Hjerm Hansen and Morten M Kramer. Modelling and control of the wavestar prototype. In *9th European Wave and Tidal Energy Conference (EWTEC), Southampton*, pages 1–10, 2011.

[52] Christian Windt, Nicolás Faedo, Demián García-Violini, Yerai Peña-Sanchez, Josh Davidson, Francesco Ferri, and John V Ringwood. Validation of a cfd-based numerical wave tank model of the 1/20th scale wavestar wave energy converter. *Fluids*, 5(3):112, 2020.

[53] Sanghwan Heo and Weoncheol Koo. Dynamic response analysis of a wavestar-type wave energy converter using augmented formulation in korean nearshore areas. *Processes*, 9(10):1721, 2021.

[54] Nathan Tom, Kelley Ruehl, and Francesco Ferri. Numerical model development and validation for the wecccomp control competition. In *International Conference on Offshore Mechanics and Arctic Engineering*, volume 51319, page V010T09A042. American Society of Mechanical Engineers, 2018.

[55] EJ Ransley, DM Greaves, A Raby, D Simmonds, Morten Møller Jakobsen, and M Kramer. RANS-VOF modelling of the wavestar point absorber. *Renewable Energy*, 109:49–65, 2017.

[56] John Ringwood, Francesco Ferri, Nathan Tom, Kelley Ruehl, Nicolás Faedo, Giorgio Bacelli, Yi-Hsiang Yu, and Ryan G Coe. The wave energy converter control competition: Overview. In *International Conference on Offshore Mechanics and Arctic Engineering*, volume 58899, page V010T09A035. American Society of Mechanical Engineers, 2019.

[57] VTI ingeniería. https://www.vtisl.com/en/test-systems/wave-laboratories/. Accessed: 2023-02-10.

[58] Palle Meinert, Thomas Lykke Andersen, and Peter Frigaard. *AwaSys 7 user manual*. Aalborg University.

[59] Speedgoat real-time target machines. https://it.mathworks.com/products/connections/product_detail/speedgoat-real-time-target-machines.html. Accessed: 2023-02-10.

[60] Charles K Chui, Guanrong Chen, et al. *Kalman filtering*. Springer, 2017.

[61] Paolino Tona, Guillaume Sabiron, Hoai-Nam Nguyen, Alexis Mérigaud, and Caroline Ngo. Experimental assessment of the ifpen solution to the wec control competition. In *International Conference on Offshore Mechanics and Arctic Engineering*, volume 84416, page V009T09A023. American Society of Mechanical Engineers, 2020.

[62] Andrew Stephen Zurkinden, Francesco Ferri, S Beatty, Jens Peter Kofoed, and MM Kramer. Non-linear numerical modeling and experimental testing of a point absorber wave energy converter. *Ocean Engineering*, 78:11–21, 2014.

[63] Antonio Falcao. Wave-power absorption by a periodic linear array of oscillating water columns. *Ocean Engineering*, 29(10):1163–1186, 2002.

[64] AD De Andrés, R Guanche, L Meneses, C Vidal, and IJ Losada. Factors that influence array layout on wave energy farms. *Ocean Engineering*, 82:32–41, 2014.

[65] Weixing Chen, Feng Gao, Xiangdun Meng, and Jianxun Fu. Design of the wave energy converter array to achieve constructive effects. *Ocean Engineering*, 124:13–20, 2016.

[66] Graham C Goodwin, Stefan F Graebe, Mario E Salgado, et al. *Control system design*, volume 240. Prentice Hall Upper Saddle River, 2001.

[67] Karl Johan Åström and Tore Hägglund. *PID Controllers: Theory, Design, and Tuning*. ISA - The Instrumentation, Systems and Automation Society, 1995.

[68] Rik Pintelon and Johan Schoukens. *System identification: a frequency domain approach*. John Wiley & Sons, 2012.

[69] KK Tan, SN Huang, and TH Lee. Robust adaptive numerical compensation for friction and force ripple in permanent-magnet linear motors. *IEEE Transactions on Magnetics*, 38(1):221–228, 2002.

[70] Dieter E Hasselmann, M Dunckel, and JA Ewing. Directional wave spectra observed during jonswap 1973. *Journal of physical oceanography*, 10(8):1264–1280, 1980.

[71] Guglielmo Papini, Francisco Javier Dores Piuma, Nicolás Faedo, John V Ringwood, and Giuliana Mattiazzo. Nonlinear model reduction by moment-matching for a point absorber wave energy conversion system. *Journal of Marine Science and Engineering*, 10(5):656, 2022.

[72] Nicolás Faedo, Fabio Carapellese, Edoardo Pasta, and Giuliana Mattiazzo. On the principle of impedance-matching for underactuated wave energy harvesting systems. *Applied Ocean Research*, 118:102958, 2022.

[73] World Marine Organization (WMO). *Guide to Wave Analysis and Forecasting*, volume 1998. 1998. ISBN 9263127026.

[74] R Kurnia and G Ducrozet. *NEMOH V3.0 User Manual*. Ecole Centrale de Nantes.
[75] Markel Penalba and John V Ringwood. Linearisation-based nonlinearity measures for wave-to-wire models in wave energy. *Ocean Engineering*, 171:496–504, 2019.
[76] Nicolás Faedo, Francisco Javier Dores Piuma, Giuseppe Giorgi, and John V Ringwood. Nonlinear model reduction for wave energy systems: a moment-matching-based approach. *Nonlinear Dynamics*, 102(3):1215–1237, 2020.
[77] Christian Windt, Josh Davidson, Pál Schmitt, and John V Ringwood. On the assessment of numerical wave makers in cfd simulations. *Journal of Marine Science and Engineering*, 7(2):47, 2019.
[78] William Finnegan and Jamie Goggins. Linear irregular wave generation in a numerical wave tank. *Applied Ocean Research*, 52:188–200, 2015.
[79] Tiago Duarte, Sébastien Gueydon, Jason Jonkman, and António Sarmento. Computation of wave loads under multidirectional sea states for floating offshore wind turbines. In *International Conference on Offshore Mechanics and Arctic Engineering*, volume 45547, page V09BT09A023. American Society of Mechanical Engineers, 2014.
[80] Michel K. Ochi. *Ocean Waves: The Stochastic Approach*. Cambridge Ocean Technology Series. Cambridge University Press, 1998.